Optical Properties and Applications of Ferrofluids—A Review

John Philip[1,*] and Junaid M. Laskar[1,2]

[1] *SMARTS, Metallurgy and Materials Group, Indira Gandhi Centre for Atomic Research, Kalpakkam 603102, Tamil Nadu, India*
[2] *Experimental Physics of Soft Matter Interfaces, Max Planck Institute for Polymer Research, Ackermannweg 10, D-55128 Mainz, Germany*

In recent years, ferrofluid has emerged as a new class of 'smart nanofluid,' whose properties are controllable by an external magnetic field. It is well known for its unique property of having both liquid and magnetic properties. Ferrofluids have been a topic of intense research during the last few decades due to their potential applications in mechanical, biomedical and optics industries. Some of the exciting applications of this material includes leak free seals, smart cooling, micro robot, micromechanical sensor, nondestructive defect sensors, tunable optical filters, actuators, optical grating, optical limiter, optical fiber modulator, magneto optical waveguide, magneto optical wavelength filter, optical switches, biosensors, hyperthermia treatment and tumor treatment, cell separation, magnetic resonance imaging based drug targeting, quantification of biomolecule agglutination etc. Besides several interesting optical effects have been observed in magnetic nanofluids under magnetic field. For example, on increasing the applied field, the transmitted intensity diminishes drastically, followed by the appearance of a 'ring' like structure in the scattered pattern, which finds applications in light limiters and switches. The scattering anisotropy factor and dipolar resonances within the scatterers are postulated as the origin for observed extinction of light. The formation of cylindrical rod-like structures, along the direction of light propagation, is manifested as a circular ring pattern in the scattered pattern. The observation of several critical fields at regular intervals in the transmitted intensity is attributed to the zippering transitions of the chains when they are in off registry. In this article, we present a critical review on various optical effects observed in ferrofluids under external magnetic field, the underlying physics and potential applications. It must be emphasized that the main focus is on scattering studies under magnetic field parallel to the incident light beam. The scattering and diffraction studies in ferrofluids (Section 4) have been elaborated for specialists.

KEYWORDS: Ferrofluids, Light Scattering, Structural Transitions, Optical Properties.

REVIEW

CONTENTS

1. INTRODUCTION

Magnetic nanofluids (suspension of fine magnetic nanoparticles with a protective layer) offer the unique possibility of tuning the particle interaction by external magnetic field that leads to interesting physical properties.[1–3] The magnetic nanofluid was first developed by NASA in the early 1960s to address the unique requirements of moving liquid fuel in a gravity-free outer-space. Development of a simple approach to tailor such fluids by chemical routes gave a major boost to the research on ferrofluids.[4–7] Ferrofluid is a unique material that has both liquid and magnetic properties, which is exploited for various applications. Figure 1 shows the photographs of a ferrofluid holding its weight on the inverted vial. On removal of magnetic field,

it flows like water. The basic constituent of ferrofluid is the magnetic nanoparticles. Transition metal oxides like maghemite (γ-Fe_2O_3) and magnetite (Fe_3O_4) are widely used in ferrofluid preparations. Maghemite has a spinel structure (space group of $Fd\bar{3}m$) and shows ferrimagnetism with a Curie temperature (T_C) of 928 K.[8] Fe_3O_4 has mixed valence of Fe^{2+} and Fe^{3+} ions and it crystallizes in cubic spinel structure with a space group of $Fd\bar{3}m$ at room temperature. These metal oxides comes under the category of spinel-type oxides with a general formula of $(M_\delta Fe_{1-\delta})[M_{1-\delta}Fe_{1+\delta}]O_4$ are technologically important class of materials.[9] Here, M is the divalent metal cation (Mn^{2+}, Fe^{2+}, Co^{2+}, Ni^{2+} and Zn^{2+} etc.) and Fe is the trivalent (Fe^{3+}) cation occupying the interstitials of FCC lattice formed by O^{2-} anions. The parenthesis and square brackets denote the *A*- and *B*-interstitial site having tetrahedral and octahedral symmetry with four and six oxygen coordination respectively. δ is inversion parameter which defines the fraction of divalent metal ion occupancy in *A* site. For $\delta = 1$ yields a structural formula of $M^{2+}[2Fe^{3+}]O_4^{2-}$ named as normal spinel, in which all the *A*-sites are occupied by M^{2+} cations and the *B*-sites are fully occupied by Fe^{3+} cations. This type of cation distribution takes place in zinc ferrites which are paramagnetic at room temperature.[10]

For $\delta = 0$, spinel structure are termed as inverse spinel having structural formula of $Fe^{3+}[M^{2+}Fe^{3+}]O_4^{2-}$. In an inverse spinel structure, all the *A*-sites are completely occupied by one half of Fe^{3+} cations and the *B*-sites are partially occupied by M^{2+} and remaining half of Fe^{3+} cations. In case of Fe_3O_4, the unit cell having a lattice constant of 8.397 Å, contains 32 oxygen anions, 64 tetrahedral and 32 octahedral interstitials sites. Out of these interstitials, 1/8 of tetrahedral (*A*-) sites are occupied by 8 Fe^{3+} cations and 1/2 of octahedral (*B*-) sites are equally shared by 8 Fe^{2+} and 8 Fe^{3+} cations. Electron hopping between the Fe^{2+} and Fe^{3+} cations in octahedral site offers the unique magnetic and structural properties of magnetite compared to other ferrites. Among iron oxides, magnetite (Fe_3O_4) is a half metallic ferrimagnet at room temperature having Curie temperature of 860 K. Fe_3O_4 and $CoFe_2O_4$ are well known examples of inverse spinel structure.

In a bulk magnetic material, each domain is separated by domain walls to minimize the net free energy of the system. Since the domain wall energy is proportional to the surface area of the particle, formation of domains becomes energetically unfavorable below critical size and form single domain size particles with giant spin called as superspin. At this critical size (D_S), sample consists of a single magnetized domain, where the system is in a

John Philip received his Ph.D. from Indian Institute of Technology, Madras in 1992 and joined IGCAR in 1996, after a post doctoral stay at CRPP-CNRS, France. Later, he also did post-doctoral reserach University of Hull, UK and ESPCI, Paris. He is currently a Associate Professor of Homi Bhabha National Institute and head of "Smart Materials and Radiation Technique (SMART) section" in Metallurgy and Materials Group of Indira Gandhi Centre for Atomic Research, Kalpakkam. He has received several awards such as Science and Technology excellence award of DAE (2006), INS medal (2007) of Indian Nuclear Society, ISNT NDT national award (2009), Ron Halmshaw award (2010) of the British Institute of Non-destructive Testing, and MRSI medal (2011). He won many international fellowships which includes Monbusho (Japan), CIES (France), Switzerland Research Fellowship. He has executed an Indo-French project on nano-emulsion during 2000–2003. He is a recipient of perspective research grant of BRNS on development of advanced nanofluids. He has six patents in his credit and over 105 publications in leading refereed international journals and 60 conference papers. He has delivered more than 50 invited lectures in India and abroad. Media (Nature, IOPnanotechweb, Hindu, Indian Express etc.) highlighted his work on several occasions. He is a reviewer of several international journals and research funding agencies in India and abroad. He is the editor-in-cheif of Journal of nanofluids of American Scientific Publishers since 2012. The research activities of Dr. Philip are in the broad area of smart nanomaterials, nanofluids, soft-matter, NDT, thermal imaging and radiography.

Junaid Masud Laskar did his Masters in Physics from Tezpur University, Assam. He is the University third rank holder for M.Sc. He joined as a research fellow in January 2006 under the guidance of Dr. John Philip and has submitted his Ph.D. thesis in 2011. The title of his thesis is "Probing of Structural Transitions in Magnetically Polarizable Soft Matters by Light Scattering." He has published eight papers in reputed international journals. He has attended six international conferences and won the best poster presentation award at Second International Conference on Frontiers in Nanoscience and Technology, Cochin. Presently, he is pursuing his post doctoral research at the prestigious Max Planck Institute for Polymer Research, Mainz, Germany.

Fig. 1. Photographs of a ferrofluid holding its weight on the inverted vial. On removal of magnetic field, it flows like water.

state of uniform magnetization and behaves like a small permanent magnet. Below the critical diameter, coercivity starts to decrease due to thermal effects. On further decrease in size, below critical superparamagnetic size (D_P) coercivity reaches zero due to rotation of particles towards the magnetic field direction spontaneously rather then the rotation of spin from one to another direction with magnetic field. Though coercivity reaches zero, $M–H$ loop of superparamagnetic particles releases energy of the order of 10^{-23} J under repeated cycle of magnetization and subsequent demagnetization which is sufficient to kill cancer cells. This particular property makes superparamagnetic nanoparticles as promising candidates for biomedical applications.[11] Magnetization of a single domain particle in thermodynamic equilibrium under the influence of magnetic field is identical to that of an atomic paramagnet except that number of atoms is of the order of 10^3–10^5, with extremely large moments and susceptibilities. Because of these resemblances, such thermal equilibrium behavior has been termed as superparamagnetism.[12] At first Frenkel and Dorfman proposed that ferromagnetic material can have a single magnetic domain below a critical size D_S. A rough estimation of the critical particle size has been made by Kittel.[13] The critical size (D_S) below which particle acts as a single domain particle is given by $D_S = 9((A_e K)^{1/2}/(\mu_0 M_S^2))$ where, A_e is the exchange anisotropy constant, K is the anisotropy constant, μ_0 is vacuum permeability and M_S represents saturation magnetization. At these critical length scales, outermost electrons of magnetic materials do not interact with each other

completely, which gives rise to new phenomena in nano-magnetism such as superparamagnetism, memory effects, size and shape dependant magnetic properties. Typical values of D_S are about 14 nm for Fe, 70 nm for Co, 166 nm for γ-Fe_2O_3, 128 nm for Fe_3O_4 and 40 nm for $CoFe_2O_4$.[14]

The tunable properties of magnetic colloidal system makes them ideal candidates for fundamental studies, besides their technological applications as biosensors, smart dampers, microfluids, optical grating, switches, filters etc.[15–21] Magnetic colloids have been used to probe interdroplet forces in presence of various stabilizing entities such as polymers, surfactants and their combinations thereof.[22–28] The magnetic colloids undergo interesting structural transitions under external fields e.g., linear chains or rods along field direction at low particle loading to complex structures such as columns, labrynthine patterns at high concentrations.[29–42] There are a few dedicated books on ferrofluids and their science and technology.[15, 43–45]

The interparticle interaction under an external magnetic field plays a prominent role on properties of magnetic nanofluids,[46, 47] which is studied both experimentally and theoretically.[48] Zahn et al. have provided experimental evidence for an enhancement of the self-diffusion function of colloidal particles at intermediate and long times due to the hydrodynamic interactions.[49] They used digital videomicroscopy to study monolayers of paramagnetic polystyrene spheres confined at air/water interface where the interparticle potential tuned by an external magnetic field. Magnetization of magnetic nanofluid as a function of field is evaluated theoretically by considering the Born-Mayer technique and expansion of dipolar coupling strength.[50] Influence of inter-particle correlations on magnetic properties of a dense magnetic nanofluid are elucidated using a statistical model.[51] Several theoretical and numerical formalisms have been developed to study magnetic colloidal interactions under different conditions.[47, 52–57] Using numerical simulation, the effects of body forces compared to the field induced forces are studied in electro-rheological and magneto-rheological fluids.[58] Experimental techniques are also developed to directly measure the forces between tiny colloidal particles.[59, 60] Interparticle interaction in magnetic nanofluid is measured experimentally by static magnetic birefringence.[61] Dependence of interparticle interaction on frequency for magnetic microspheres is studied, by floating the two microspheres on glycerin and applying ac magnetic field.[62] Room temperature ferromagnetic resonance is used to investigate particle–particle interaction in magnetic nanofluid.[63] From the variation of the blocking temperature of magnetization curve, the interparticle interaction for a magnetic nanofluid is measured experimentally.[64] The non magnetic interaction, termed as field induced structural force is found to play an important role in the aggregation of particles in polydisperse ferrofluid.[65]

The measurement of dynamic magnetic behavior of magnetic nanofluid shows that unlike the superparamagnetic

behavior at room temperature, at low temperatures the magnetization has a hysteresis loop that is attributed to Neel relaxation processes.[66] The magnetic remanence increases with the decrease in temperature and increase with the frequency of magnetization field. The critical exponents in a dipole–dipole interacting magnetic nanoparticles in a concentrated frozen magnetic nanofluid have been determined using static scaling analysis of the nonlinear susceptibility measured experimentally.[67] A phenomenological model to describe magnetodynamics of spherical nanometer sized particles is developed by assuming that at low temperatures the magnetization is weakly pinned at the particle surface by a unidirectional anisotropy.[68] By fitting the ferromagnetic resonance spectra, the surface anisotropy constant for maghemite nanoparticles constituting ionic ferrofluids is evaluated. The experimental magnetization curves of polydisperse magnetic nanofluids are analyzed using second order modified mean field theory.[69] Molecular dynamics and Monte Carlo simulations performed on systems possessing prescribed magnetic-core diameter distributions show perfect agreement between theory, simulation and experiment. The DC magnetization, AC susceptibility, and hyperthermia characteristics of different ferrofluids are measured to study the magnetic relaxation and dissipative heating.[70] Ferrofluids show a clear Néel relaxation, but on studying the magnetic dissipation near the freezing temperature, it is observed that Brownian relaxation is only significant for the isolated nanoparticle samples, Fe_3O_4 and γ-Fe_2O_3 based nanofluids, while the nanoparticles in alginate hydrogel, show a minimal Brownian relaxation. In the measurement of magneto-rhelogical properties of a suspension of nonmagnetic particle in a magnetic nanofluid, the storage modulus is found to be an order of magnitude larger than the loss modulus.[71] The storage modulus depends weakly on the frequency but varies linearly with the volume fraction of the sample. The increase in viscosity of a ferrofluid due to an applied magnetic field is discussed on the basis of a phenomenological relaxation equation for the magnetization.[72–74] The role of dipolar interactions on viscosity of magnetic nanofluids under magnetic field is evaluated by molecular simulations and dynamical mean-field theory.[75] The refractive index of a magnetic nanofluid increases with the increasing field strength over a critical field, and then becomes saturated as the field reaches another critical value.[76] At higher temperatures, the refractive index under an external field is found to reduce.[77] The variation in the refractive index of magnetic nanofluid film with rising field strength is enhanced by increasing either the concentration or the film thickness, or by applying the field along the film surface, whereas it is independent on the sweep rate of the field.[78] The magnetic nanofluid doping, even in small quantities, modifies the nonlinear response (refractive index) of the lyotropic phase of liquid crystal, as measured by transmission Z-scan technique.[79] It is shown that hydrodynamic Maxwell theory gives a better and correct estimate of electromagnetic fields

in a dielectric magnetic nanofluid than linear response theory.[80, 81] Magnetic nanofluid exhibits different magneto optical properties such as field birefringence, linear dichroism, Faraday rotation, Faraday ellipticity and circular dichroism.[82–85] The temperature and field dependent study in a water-based magnetic nanofluid shows that the specific heat is almost independent of temperature under lower-field strengths, but decreases significantly upon increasing temperature under higher fields.[86] Large enhancement and tunable thermal conductivity for magnetite nanofluids along the external magnetic field, which is parallel to the temperature gradient, is observed recently.[2, 7, 73] Bulk flow of a magnetic nanofluid in a uniform rotating magnetic field is obtained directly using the ultrasonic velocity profile method.[87] The fluid is observed to co-rotate with the field in a rigid-body like fashion throughout the container, except near the air-fluid interface, where it is observed to counter-rotate. Brownian dynamics simulations study, of anisotropic self-diffusion in magnetic nanofluids in the presence of a magnetic field, shows that the diffusion parallel to the magnetic field is hindered compared to the case without field.[88] Depending on the strength of dipolar interactions, the diffusion perpendicular to the applied field is either enhanced or hindered due to the field. The average diffusion coefficient is found to decrease with increasing concentration and dipolar interaction strength, but is independent of the magnetic field strength for moderate dipolar interactions. Odenbach has extensively studies the flow properties of magnetic nanofluids with and without magnetic fields.[89–92]

The unique interparticle interaction and unusual properties in the magnetically polarizable soft matter give rise to interesting observable physical phenomena. Magnetic nanofluids are used to reduce the strength of magnetic field required to orient the nematic liquid crystals.[93] Glassy behavior is observed in a frozen magnetic nanofluid due to dipolar interactions and is found to deviate from canonical spin glasses.[94, 95] Spin glass dynamics is observed in very concentrated frozen ferrofluid, whereas the dilute system shows isolated particle dynamics.[96] Analytical and numerical studies of the evolution of a magnetic nanofluid drop, confined to a rotating Hele-Shaw cell in the presence of an azimuthal magnetic field, demonstrates that the centrifugally driven interfacial fingering instabilities can be simply controlled with the use of a current-carrying wire.[97, 98] Non linear phenomena such as parametric stabilization of Rosensweig instability,[43, 99] generated by vertical vibration of fluid container is observed in magnetic nanofluid.[100] Rayleigh-Taylor (RT) instability, a gravitational instability that occurs when a dense fluid lies above a less dense fluid causing fingering at the interface between the fluids, is observed experimentally by controlling the external magnetic field and analyzed well theoretically, when one of the fluids is magnetic nanofluid or magnetorheological fluid.[101–103] Experimental study of a fingering pattern formation, which occurs during the spreading of

an immiscible thin ferrofluid drop subjected to a radial magnetic field, is reported.[104] Another type of remarkable patterns is associated with the so called labyrinthine instability,[101, 105–107] where highly branched structures are formed when a ferrofluid droplet is trapped in the effectively 2D geometry of a Hele-Shaw cell.[108] under a perpendicular uniform magnetic field. The relaxation of an asymmetric magnetic nanofluid drop, subjected to a homogeneous alternating magnetic field, gives rise to translational motion, which can be used to build liquid motors.[109] It is experimentally demonstrated that in the case of magnetic nanofluid, the force exerted by the external electric and magnetic field is not of Kelvin's force observed in neutral dielectric body.[110] Standing waves of superlattice, rhombus, square and hexagonal shapes are observed on the surface of magnetic nanofluids driven parametrically with an ac magnetic field. It is argued that the superlattice pattern is formed by the resonance of newly generated sub harmonic modes with the harmonic hexagonal modes already present.[111] Magnetic nanofluids are also shown to be a model system to demonstrate and investigate thermal ratchet behavior, an interesting phenomenon of statistical physicsists.[112] Spatio-temporal intermittency, studied in the context of hydrodynamics and characterized by patches of ordered and disordered states fluctuating stochastically in space and time, is observed and investigated in a system consisting of a ring of spikes excited on magnetic nanofluid surface by an external magnetic field.[113] Stable soliton-like structure is observed on the surface of a magnetic nanofluid, generated by a local perturbation in the hysteretic regime of the Rosensweig instability.[114] The radioscopic measurements of the soliton's surface profile suggest that locking on the wavelength defined by the non-monotonic dispersion curve is instrumental in soliton's stabilization. Depending on the ratio of magnetic and capillary forces, both elevation and depression axisymmetric solitary waves are observed on the surface of a cylindrical magnetic nanofluid layer surrounding a current-carrying metallic tube.[115] The profiles of these solitary waves are in good agreement with theoretical predictions based on the magnetic analogue of the Korteweg–de Vries equation.[116] The measured velocity and dispersion relation of these axisymmetric linear waves propagating on the cylindrical magnetic nanofluid layer are found to be in good agreement with theoretical predictions. Dipolar chains of nonmagnetic particles in a suspension of magnetic nanofluid fluctuate under the effect of Brownian noise at equilibrium, and these dipolar chains roughen dynamically on sudden decrease of external magnetic field.[117] On studying the time and size scaling of the chain fluctuations, roughening, and the relationships between the equilibrium and out of equilibrium behavior, it is shown that this phenomenon can be described equivalently as a non-Markovian anomalous diffusion process for a particle in systems with memory. Transition from an ordered solid-like phase to a disordered liquid-like phase of a lattice of spikes is observed

on a magnetic nanofluid surface submitted to horizontal sinusoidal vibrations.[118] The melting transition occurs for a critical spike displacement which is experimentally found to follow the Lindemann criterion, the critical root mean square (rms) value of the spike displacement at the melting transition is given by a constant fraction of the spike-to-spike distance, for two different lattice topologies (hexagonal and square) and over a wide range of lattice wavelengths. This dissipative out-of-equilibrium system exhibits strong similarities with 2D crystal melting in solid-state physics. Wave turbulence is observed on the surface of a ferrofluid mechanically forced and submitted to both static normal.[119] and parallel.[120] magnetic fields. Optical negative refraction is demonstrated numerically in magnetic nanofluid containing isotropic Fe_3O_4 nanoparticles, having Ag shell, in the presence of an external DC magnetic field.[20] The all-angle broadband optical negative refraction, controllable by external magnetic field, arises from the field induced chains or columns.

2. LIGHT SCATTERING STUDIES

Besides probing the field induced structural transitions in ferrofluid, ferrofluid emulsion and mixed magnetically tunable soft systems are studied using light scattering where several interesting scattering phenomena are also observed.[19, 42, 121–127] The desire to use and control electromagnetic waves in strongly scattering media in a manner analogous to the control of electrons in condensed matter has inspired great interest in topics such as the localization of light, coherent backscattering, microcavity quantum electrodynamics, near-field optics, photonic magnetoresistance and anisotropic diffused coefficients etc.[128–135] Observation of photonic Hall effect is reported for the first time, both theoretically and experimentally, in magnetic nanofluid.[136] Disappearance of forward and backward scattered light is observed at a certain critical magnetic field for a system containing micron sized magnetic spheres dispersed in magnetic nanofluid. The critical field is found to depend on the concentration of ferrofluid and the volume of the magnetic spheres.[137, 138] Upon increasing the field from this critical value, an enhancement in the backscattered intensity is observed. Significant increase of the optical attenuation length along the field direction in suspension of magnetic particles as a function time, enhancement of non linear optical properties etc. are also observed in these systems.[42, 123, 139–144]

For very small particles much less than the light wavelength, the turbidity of colloidal suspension increases substantially due to aggregation and this aspect has been used to measure the aggregation rate and stability. Light scattering is also used to probe the aggregation kinetics of magnetic colloidal systems.[145, 146] In magnetic emulsion, the field induced structural transition is investigated measuring transmitted light intensity. Aggregation times at different external fields are elegantly probed from the variation

of forward scattered light and the scattered pattern.[126] Also, aggregation rate at different external magnetic fields is found by measuring both the scattered light at small angle[147] and transmitted light.[148] Due to various structural transitions under external magnetic field, interesting phenomena resulting from light scattering in magnetic colloidal systems are observed. Dramatic increase of the optical attenuation along the field direction in suspension of magnetic particles,[139] photonic Hall effect in liquid and gelled samples of ferrofluid,[136] vanishing of both forward and backward scattered light from a dispersion of micron sized magnetic particles in a ferrofluid above some critical magnetic field[137, 138] etc. are to name a few. Other phenomena of scattering and diffraction of light in magnetic suspensions, emulsions and mixtures of magnetic and nonmagnetic scatterers have also been investigated both theoretically and experimentally.[149–152]

When the size of particles or droplets of magnetically tunable soft matters are in the nano range ($d < 10$ nm), where d is the particle diameter; the challenge in studying structural transitions and their kinetics *in situ* under external field increases manifold because of the limited available experimental tools. For very small particles with their sizes (d) much less than the light wavelength (λ) i.e., $d \ll \lambda$, the turbidity of colloidal suspension increases substantially due to aggregation. Though this particular aspect has been exploited to measure the colloidal aggregation rate and the stability in non magnetic systems,[153] it is not used for the magnetic ones. Though there have been a few studies on scattering of light in magnetic soft matters, in the size limit $d \gg \lambda$, scattering in the limit $d \ll \lambda$ is not investigated thoroughly. Magnetically tunable soft matters are excellent model systems to study the scattering phenomena in different regimes because the scatterers' sizes can be tuned from Rayleigh regime ($d \ll \lambda$) to Mie regime ($d \sim \lambda$) and finally to the geometrical regime ($d \gg \lambda$) by simply changing external magnetic field. Due to the complex field induced structural transitions, the magnetically tunable soft matter systems also turn out to be ideal system to study electromagnetic wave scattering and propagation through ordered, weakly ordered media and during order-disorder transition.

The full understanding of the structure, phase behavior, and aggregation kinetics of strongly interacting dipolar magnetic fluids is still incomplete. The form of interaction energy between two field induced chains of magnetorheological colloids as function of distance is always attractive in nature for head to tail aggregation whereas for lateral aggregation has a repulsive component as well.[37] Using analytic and numerical approaches, it has been speculated that column sizes seen in the experiments are not the true representation of the equilibrium structure.[154] True experimental results that describe equilibrium phenomena from metastable state are still unclear. Irrespective of some systematic studies on structural transition kinetics in magnetic colloids, understanding of the underlying

mechanism for aggregation time is still in an infancy.[155] In all the structural transition kinetics studies carried out so far, both theoretical and experimental, the aggregation process is studied as a function of time for different external field strength or concentration of the colloidal system.[31, 126, 145–147, 155–169]

Most of the unusual properties of magnetically tunable soft matter originate from conformation of particles and structural transitions that occur under external magnetic field. Therefore, it is important to have in an in-depth understanding of these complex structural transitions, their kinetics and the interactions governing these transitions under various external conditions. In the presence of an external field, the particles in magnetic colloids experience attractive force along the field direction and a repulsive force normal to it. At first, the randomly oriented dispersed Brownian particles undergo head to tail aggregation forming chains aligned along the field direction. Due to the lateral coalescence of the chains, they form columns by undergoing secondary aggregation.[31, 33] Therefore, the dipolar colloidal system undergoes interesting structural changes under external field leading to interesting structures that includes linear chains or rods, columns, labrynthine patterns etc.[29–40, 170–174]

3. APPLICATIONS OF FERROFLUID

Due to the external field tunability of their properties, applications of magnetically tunable soft matters are increasing everyday.[175, 176] They find applications in various branches of mechanical engineering, optical engineering and biotechnology.[177] Magnetic nanofluids are being used in smart cooling,[2, 3] micro robot,[178] micromechanical sensor,[179] nondestructive defect sensors,[180, 181] tunable optical filters,[17] hydrostatic bearing,[182] microfluidics,[183, 184] actuator,[185] liquid seal,[186] optical grating,[187] optical limiter,[188] optical fiber modulator,[16, 189] magneto optical waveguide,[190] magneto optical wavelength filter,[191, 192] optical switches,[18] biosensors,[193, 194] hyperthermia treatment,[195, 196] tumor treatment,[197] cell toxicity study,[198] magnetic resonance imaging based drug targeting,[199] quantification of biomolecule agglutination,[200] imaging[201] etc. Here, we discuss some of the most recent applications of ferrofluids, as the old ones were already been covered in the earlier reviews. For imaging internal defects in materials, a magnetically polarizable nanoemulsions are used.[181] It has been shown that the gradient in the magnetic flux lines around the defective region leads to the formation of one-dimensional (1-D) nanodroplet arrays along the field direction, which incredibly diffract the incident white light to produces bright colors where the diffracted wavelength has a direct correlation with the defect features. Figure 2 shows the color pattern observed on sensors, placed on specimens with (b) two adjacent circular holes and (a) with a cylindrical hole and circular hole buried inside the sample. This
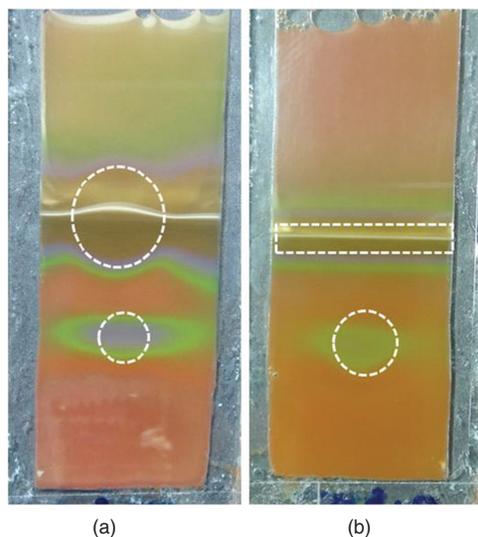
Fig. 2. The color pattern observed on ferrofluid sensors, placed on specimens with (a) two adjacent circular holes and (b) with a cylindrical hole and circular hole buried inside the sample.

approach enables visual inspection of ferromagnetic components and has several advantages over existing flux leakage sensors in terms of cost, re-usability of the sensor and complexity. The tunable thermal property of a magnetically polarizable nanofluid that consists of a colloidal suspension of magnetite nanoparticles of average diameter 6.7 nm is exploited for smart cooling applications.[2] Controlling the linear aggregation length from nano to micron scales, the thermal conductivity of the nanofluid has been enhanced up to 216%, using 4.5 vol.% of nanoparticles. Repeated magnetic cycling shows that the thermal conductivity enhancement is perfectly reversible. The large enhancement in thermal conductivity is attributed to the efficient transport of heat through percolating nanoparticle paths.

Optical filters are used to select different wavelengths of light. Color imaging systems benefit from the use of precision optical filters, which control the spectral properties of light and color separation to exacting tolerances. In spectroscopic and interferometric experiments, involving different wavelengths of light, different types of interference filters are required to eliminate stray light entering the detector head. In those experiments, filters are to be replaced, whenever the light source (wavelength) is changed. The replacement of filters is cumbersome, especially when the wavelength is changed continuously with tunable type of lasers. In order to avoid the problems mentioned above a novel tunable optical filter using ferrofluid emulsion is developed.[17] The filter comprises of ferrofluid-based emulsion cell, a miniature solenoid and a variable direct current source for changing the magnetic field. By varying the magnetic field, desired wavelength is selected. The main advantage of the new optical filter is that a single filter can be used for a range of central

wavelengths, where the desired central wavelength region can be tuned by external magnetic field.

Brousseau et al. have developed an innovative low-cost deformable mirror made of a magnetic liquid (ferrofluid) whose surface is actuated by an hexagonal array of small current carrying coils.[202, 203] They compared the theoretical and experimental performances of a 37-actuator ferrofluid deformable mirror along with wavefront correction examples. They showed the validity of the model used to compute the actuators currents to obtain a desired wave front shape. Later the same group has demonstrated linearization of the response of a 91-actuator magnetic liquid deformable mirror too.[204]

Kurlyandskaya et al. have shown magneto impedance effect in a $Co_{67}Fe_4Mo_{1.5}Si_{16.5}B_{11}$ amorphous, ribbon-based sensitive element, in the presence of a commercial ferrofluid thin layer covering the ribbon surface.[205] The magneto impedance response is found to dependent on the presence of the magnetic ferrofluid and applied magnetic field. and the parameters of the driving current. Authors proposed applications in fabrication of biomaterials with a high level of affinity and specificity as bimolecular labels. Pekas et al. integrated giant magnetoresistance (GMR) sensors with a microfluidic system for the velocity and size monitoring, and enumeration of flowing magnetic entities.[183] Their system enabled controlled formation of picoliter-sized droplets of a ferrofluid separated by a non-magnetic oil; and the continuous-flow sensing of these ferrofluid droplets.

Horng et al. have demonstrated that designing a refractive index by using magnetic fluids, around 1.465 at 1.557 μm wavelength, which may find applications in optical fiber communication.[206] They also showed a methodology to achieve a desired flexibility in the tunable refractive index with externally varying fields by adopting suitable magnetic fluid films suitable for index-match or index-tunable devices.

The same group has demonstrated a magnetic-fluid-based optical switch that is formed by sealing magnetic fluid between two glass prisms.[18] They observe that when a light is incident to one side of one of the prisms, a reflected light from the magnetic fluid film comes out from the same prism, whereas a transmitted light through the film emits from the other prism. Therefore, the intensity ratio of the reflected light to the transmitted light is manipulated by varying the external magnetic field strength. The switching efficiency was found to depend on the incident angle of a light into the prism. Horng group has further developed an optical-fiber modulator using magnetic fluid as a cladding layer by applying magnetic fields to reduce the optical-fiber modulator transmission.[16] They observe that the magnetically induced transmission loss of an optical-fiber modulator under external magnetic fields is dominated by the number of magnetic clusters in the cladding magnetic fluid and that the formation of magnetic clusters depends on the length of the fiber modulator.

REVIEW

Li et al. have also observed that the intensity of light transmitted through a thin ferrofluid film could be modulated by an applied magnetic field.[143] Horng group has also developed a novel a platform for wash-free immunomagnetic detections.[207] Liu et al. have proposes a magneto-optical tunable filter based on a long-period fiber grating coated with magnetic fluids.[191]

Patel et al. have shown that magnetic field induced extinction of light and birefringence as a function of temperature can be used to study the temperature dependence of magnetic moment as well as the domain magnetization of the temperature sensitive magnetic fluids.[208] Song et al. demonstrated a simple method to manipulate free microdroplets using ferrofluid dynamics.[209] For droplet transport, they used a set of periodic lines of ferrofluid on top of a silicon wafer by a single strip magnet and dynamically changed by the rotation of a magnetic stirrer underneath it. It has been found that the speed of droplet movement depends on the rotation speed of the magnetic stirrer as well as the size of the droplet. Nair et al. have studied the optical limiting properties of ferrofluids using nanosized particles of approximately 80 Å diameter.[188] They studied the nonlinear optical transmission of the samples using nanosecond and femtosecond laser pulses.

Whitesides group has developed a methodology for fabrication and use of a three-dimensional magnetic trap for diamagnetic objects in an aqueous solution of paramagnetic ions where the trap uses permanent magnets.[210] They elegantly demonstrated trapping of polystyrene spheres, and of various types of living cells: mouse fibroblast sNIH-3T3d, yeast (Saccharomyces cerevisiae), and algae (Chlamydomonas reinhardtii). Pu et al. have developed a tunable magnetic fluid grating where they observe the energy of the zeroth-order diffracted light is transferred to that of the higher-order completely and vice versa when the absorption coefficient modulation of the grating is not too large.[187] They have also shown a simple method based on the retroreflection on the fiber-optic end face to measure the refractive index of a magnetic fluid.[211] Further they have also shown a method for suppressing the thermal lens effect in a magnetic fluids.[212] They observe that, the thermal lens effect is weakened, and the degree of the divergence of the laser beam after passing through the magnetic fluid decreases when an external parallel magnetic field is applied.

Hong et al. have shown a method to synthesizing biofunctionalized magnetic nanopaticles for the purpose of magnetically labeling biomolecules and a system to measure the ac magnetic susceptibility of the labeled sample.[213] They have found that when a targeted biomolecule was mixed with magnetic fluid possessing biofunctionalized magnetic nanoparticles, portions of magnetic nanoparticles agglomerated to form clusters due to the association with the targeted biomolecule, which lead to the reduction in the ac magnetic susceptibility.

Guo et al. exploited the movement of ferrofluid droplets on superhydrophobic surfaces in the presence of strong external magnetic fields that allowed the quantitative evaluation of friction between droplet and substrate surface.[214] This approach enabled the development of microferrofluidic devices and in the remote actuation of droplets on surfaces, which was not possible using conventional microfluidics, inkjet printing, electro-wetting, or light-driven motion. Chung et al. have experimentally demonstrated a biomagnetic sensor scheme based on Brownian relaxation of magnetic nanoparticles suspended in liquids.[194] They showed that the characteristic time scale of the Brownian relaxation is determined directly by ac susceptibility measurements as a function of frequency where the peak in the imaginary part of the ac susceptibility shifts to lower frequencies upon binding the target molecules to the magnetic nanoparticles.

Inglis et al. demonstrated a continuous-flow microfluidic device that enables cell by cell separation of cells selectively tagged with magnetic nanoparticles.[184] They showed that the cells flow over an array of microfabricated magnetic stripes, which create a series of high magnetic field gradients that trap the magnetically labeled cells and alter their flow direction, which was observed in real time using a low power microscope and the device has been demonstrated by the separation of leukocytes from whole human blood. Choueikani et al. have developed magneto-optical waveguides made of cobalt ferrite nanoparticles embedded in silica/zirconia organic–inorganic matrix.[190] Wang et al. have recently studied the structural force arising from magnetic interactions in polydisperse ferrofluids.[65] The unusual green color observed in magnetite hollow spheres is interpreted in terms of the Mie scattering on the inhomogeneous and low-density structure of the hollow spheres with a characteristic diameter that is comparable to the wavelength of the visible light.[215]

4. FIELD INDUCED STRUCTURAL TRANSITIONS STUDIES

4.1. Techniques Employed for Structural Transition Studies

Various techniques have been employed to get insight into the field induced structural transitions and their kinetics of magnetic nanofluids.[29, 122, 164, 167] Among these, light scattering studies has been extensively used as a diagnostic tool to probe the structural transitions and their kinetics in magnetic soft matter systems under external field. X-ray scattering,[122, 216] Small Angle Neutron Scattering (SANS),[217–221] Small Angle X-ray Scattering (SAXS),[218, 220, 222] time-resolved stroboscopic SANS[169] etc. have also been used to get insight into the structural transitions of various magnetic colloidal systems under external magnetic field. The simulation of magnetic or other dipolar fluids using Monte Carlo (MC) methods

has been employed for the last three decades in order to extract information on structure formation in such systems. Because of the limited computer capacities, the early investigations were performed on two-dimensional models.[156, 223–225] Later, MC simulations are extended to three dimensions for both monodisperse[157, 226–233] and polydisperse[234, 235] systems to study the field induced structural transitions and their kinetics. Time dependent structural evolution in magnetic soft matter system is also studied by molecular dynamics,[1, 164, 236] stochastic dynamics,[165] Brownian dynamics,[166] model based computer simulation.[167] Using both static and video optical microscopy, the field induced structural transitions (chains, columns etc.) and their kinetics are studied in different magnetic soft matter systems such as dispersion of paramagnetic latex particles, ferrofluid emulsions, sulfonated polystyrene particles with iron oxide in water, magnetic nanofluid etc.[29–31, 33, 36, 39, 145, 155, 156, 158–161, 237, 238] The optical microscopy technique has been particularly successful when the aggregating entities are in the optical resolution range (> 200 nm). In magnetic nanofluid, the dispersed particles are very small (~ 8 nm), therefore it is beyond the resolution limit of optical microscope. Even though there have been few efforts using Cryo Transmission Electron Microscopy (Cryo-TEM),[40, 239, 240] *in situ* study of field induced structural transition in magnetic nanofluid still remains as a challenge. Light scattering with electron microscopy is used to probe the field induced structural transition kinetics of magnetic soft matter systems.[146] Scattering dichroism[163] and Raman spectroscopy[168] are also employed to obtain insight into the structural transition dynamics for different magnetic colloidal systems. In ferrofluid emulsion, the field induced structural transition is investigated by measuring the transmitted light intensity.[39] Aggregation times at different external fields are elegantly probed from the variation of forward scattered light and the pattern.[126] Also, aggregation rate at different external magnetic fields is found by measuring both the scattered light at small angle[147] and transmitted light.[148]

The nanoparticles in magnetic colloids are in random thermal Brownian motion in the absence of external magnetic field. On application of external magnetic field, each individual particle acquire dipole moment of the magnitude given by

$$m = \frac{4}{3} \pi a^3 \chi H_0 \tag{1}$$

where a is the radius of the particle, χ is the magnetic susceptibility and H_0 is the magnitude of external magnetic field. This causes the moments of the particles to align along the field direction and also increases the anisotropic interaction energy between two such particles, given by[37]

$$U_{ij}(r_{ij}, \theta_{ij}) = \frac{m^2 \mu_0}{4\pi} \left(\frac{1 - 3\cos^2 \theta_{ij}}{r_{ij}^3} \right) \tag{2}$$

where r_{ij} is the position vector of ith particle relative to the jth particle and θ_{ij} is the angle between the external field

and the position vector. As the particles are in Brownian motion, the effective interaction between them can be described by a coupling constant (Λ) which is the ratio of the maximum magnitude interaction energy to the thermal energy ($k_B T$) in the system

$$\Lambda = \frac{\pi \mu_0 d^3 \chi^2 H_0^2}{72 k_B T} \tag{3}$$

Here, k_B is the Boltzmann constant, T is the temperature and d is the diameter of the particle. When $\Lambda \geq 1$, the particles in the dispersion self assemble to form one dimensional chain like structures along the field direction. The *in situ*-cryogenic transmission electron microscopic observations of magnetite nanoparticles dispersions under magnetic field confirms columnar structures exhibiting distorted hexagonal symmetry.[40] Also, such field induced ordering is observed in aqueous ferrofluids.[36] In the next Sections 4.2–4.6, we review specific studies on field induced structural transitions in ferrofluids carried out in authors laboratory.

4.2. Samples Used for Scattering Studies

The experiments are performed in a stable colloidal system of magnetite (Fe_3O_4) particles coated with oleic acid and dispersed in a hydrocarbon carrier fluid. Average diameter of the particles and organic layer thickness around the particles are 6.7 nm and 1.5 nm respectively. The complexities originating from electrostatic interactions between the nanoparticles are eliminated by using a non-aqueous magnetic nanofluid. Measurement of transmitted light intensity and recording of the scattered pattern as a function of magnetic field are carried out to study the aggregation process in the system using a fully automated light scattering set up shown in Figure 3. An amplitude and frequency stabilized polarized He–Ne laser (Spectra-physics) of wavelength (λ) 632.8 nm with an output power 1 mW is used as the light source. The propagation wave vector of incident light is parallel to the external field direction. The applied magnetic field is varied by using a programmable current source and a solenoid, inside which the sample is placed in a sealed a quartz cuvette. Transmitted light intensity is measured using a photomultiplier tube (PMT Oriel)
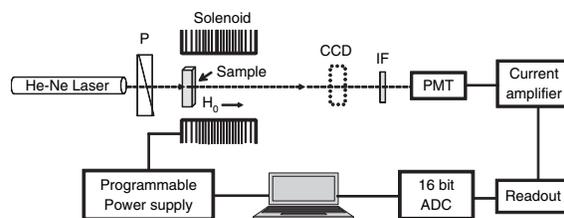

Fig. 3. Schematic of the experimental set up. The direction of the applied magnetic field is along the direction of propagation of the beam. *P*-polarizer and IF-interference filter.

and its output is fed to readout through a current amplifier with variable gain. The analog output from the readout is connected to a 16 bit ADC that is interfaced with a computer. The scattered pattern, observed on a screen is recorded using a CCD camera. The variation in the magnetic field within the sample was less than 1% and the variation within the laser spot diameter was less than 0.01%.

To carry out time dependent light scattering measurements the following experimental procedure is adopted. Magnetic field is increased in steps of 6.43 Gauss. After each increment, the intensity is measured for 120 seconds. If there is no intensity variation within this time, the field is increased to another value. If intensity varies, then it is measured as function of time till it reaches a stable value. The pattern of the scattered light is also recorded using a CCD camera.

4.3. Variation of Transmitted Light Intensity as a Function of Applied Field

Figure 4 shows the normalized transmitted intensity as a function of external field for different magnetite volume fractions. The intensity plotted is the ratio of the intensity transmitted through the sample with and without magnetic field. Here, at lower concentrations, the transmitted light intensity remains constant upto a 'critical' magnetic field (H_{C_1}) above which the intensity starts to decrease drastically. At another 'critical' magnetic field named as H_{C_2} the transmitted light intensity becomes a minimum. Above H_{C_2}, the transmitted light intensity increases slowly. Also, with increasing concentrations, the slope of the transmitted intensity curve (between H_{C_1} and H_{C_2}) increases. At higher particle concentrations above 0.0176 volume fraction, the transmitted light intensity at first increases slightly and then decreases with increasing in magnetic field.
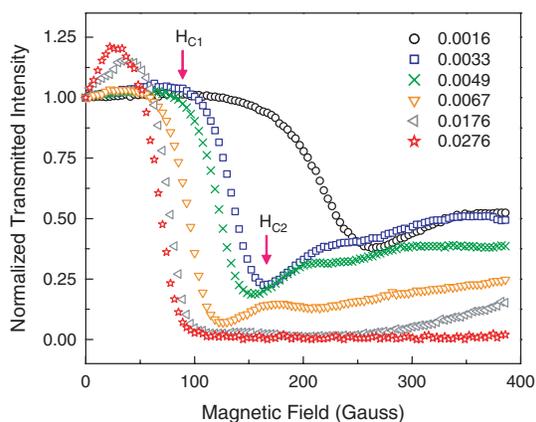
To assess the effect of volume fraction (ϕ) of nanoparticles on the critical magnetic field, the variation of the critical fields H_{C_1} and H_{C_2} as a function of volume fraction of the nanoparticles are plotted as shown in Figure 5. Both H_{C_1} and H_{C_2} follow power law decay with volume fraction ($H_C \propto \phi^{-x}$) where the exponents are 0.423 and 0.283 respectively. The scaling analysis also predicts such power law dependence where exponents can vary between 0.25 and 0.75 for structural transitions in ferrofluid emulsion under external magnetic field.[39]

The forward scattering patterns from a magnetite suspension ($\phi = 0.0067$) at various magnetic fields are shown in Figure 6. Here, the transmitted light intensity drops to zero at a magnetic field strength of 115 Gauss, above which the forward scattered light shows a diffused ring like structure i.e., when the applied magnetic field is above H_{C_2}. The ring becomes sharper as the magnetic field strength increases. It should be noted that the spot appears at the same place at different magnetic fields. However, the spot size decreases as the magnetic field strength is increased.

What are the possible reasons for the observed extinction of light at H_{C_2}? The absorption study in kerosene based ferrofluid in the visible range (400–800 nm) shows no characteristic visible absorption peak around 632.8 nm (for particle size of 10 nm, $\phi = 0.036$; path length 10 mm, the absorbance was 0.015).[241] As the wavelength of the laser light that is used for the experiment is 632.8 nm, and the volume fraction is much lower than the above case, the extinction of light cannot be due to absorption. Of course, there is no reason for the light to be absorbed at a feeble magnetic field strength of 0.02 T. Therefore, this possibility is also ruled out. Can this light extinction be due to the dynamics of nanoparticles during the field induced ordering? In ferrofluids, nanoparticles are usually smaller than domain size and are free to rotate independently from

Fig. 4. The normalized transmitted light intensity as a function of applied magnetic field for magnetite based ferrofluid of different volume fractions (ϕ). Reprinted with permission from [41], J. M. Laskar, J. Philip, and B. Raj, *Phys. Rev. E* 78, 031404 (**2008**). © 2008, American Physical Society.
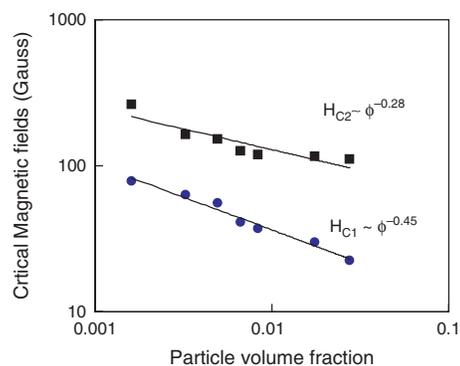
Fig. 5. The critical magnetic fields (H_{C_1} and H_{C_2}) as a function of magnetite volume fraction (ϕ). The critical fields H_{C_1} and H_{C_2} follow power law decay with volume fraction ($H_C \propto \phi^{-x}$) where the exponents (x) are 0.423 and 0.283 respectively. Reprinted with permission from [21], J. Philip, J. M. Laskar, and B. Raj, *Appl. Phys. Lett.* 92, 221911 (**2008**). © 2008, American Institute of Physics.
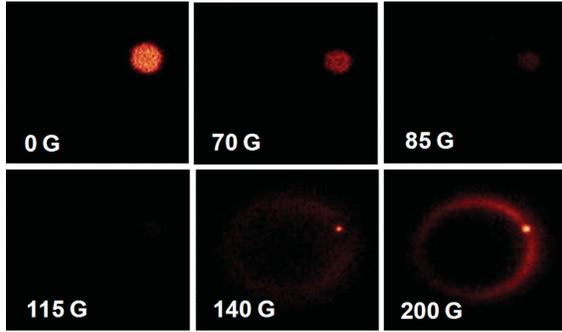
each other. Brownian motion and Neel rotation are the relaxation mechanisms due to particle and spin rotation respectively.[169] The relaxation time for Brownian motions given by $\tau_B = (3V'\eta)/(k_B T)$, where V' is the hydrodynamic volume of the particle and η is the dynamic viscosity. Neel relaxation is attributed to the rotation of the moment in the particle with a relaxation time given by $\tau_N = \tau_0 \exp((KV')/(k_B T))$, K is the anisotropy constant, τ_0 typically of the order of a few nanoseconds. For a particle of 10 nm size, the value of τ_N and τ_B are 10^{-9} s and 7.6×10^{-7} s respectively. However, the value of τ_N increases sharply with the size of the particle due to the exponential dependence on V'. The time dependent transmission measurement at different rate of application of magnetic fields shows 100–180 sec for a complete recovery from the extinction. Therefore, the internal dynamics should not be the origin for the observed extinction.

Another mechanism for the decrease of transmitted light is the optical limiting of laser light from a colloidal suspension of spherical particles.[242] This limiting has been shown to be mainly due to nonlinear light scattering by the two component colloidal suspension system. However such enhanced nonlinear light scattering takes place only at high fluences due to the photo induced mismatch of the refraction indices of the two components in colloidal suspension. Since the incident laser light intensity is very small (1 mW), the above mentioned possibility of nonlinear light scattering due to photo-induced refractive index mismatch between the two components of the suspensions is ruled out.

Christiansen has shown that in small grains of particle suspensions, the dispersion curves can coincide at one wavelength.[243, 244] However, at 632.8 nm, the refractive indices of dispersed magnetic nanoparticles and dispersion medium kerosene do not coincide. Therefore, the possibility of the decrease of light due to Christiansen effect is also ruled out. Kerker's theory deals with the scattering of light by magnetic spheres.[149] Considering magnetic permeability $\mu \neq 1$ in the small particle (or long wavelength)

limit, the condition for the two polarized components of scattered radiant intensity with electric vectors perpendicular and parallel to the scattering plane are derived and given as

$$\varepsilon = \frac{(4-\mu)}{(2\mu+1)} \quad (4)$$

In our experiments, is it possible to fulfill the Kerker's condition for zero forward scattering at $a \ll \lambda$ as suggested recently?[137, 138] The light ($\lambda = 632.8$ nm) that is incident and gets scattered from the Fe_3O_4 nanoparticles in the dispersion is in the visible range of the spectrum for which magnetic permeability value $\mu = 1$. Since, Kerker's condition (Eq. (4)) is derived for frequencies lower than optical frequency, it cannot be applied in our case.

What could be the reason for the observed extinction? For a disordered medium of identical spherical particles (here considered as scatterer) of radius a, illuminated by light of wavelength λ, the localization parameter kl^* depends on the scatterer's magnetic permeability μ, where $k = (2\pi N)/\lambda$ is the wave vector, $l^* = l/(1 - \langle \cos\theta \rangle)$ is the transport mean free path, N is the refractive index of the medium.[150, 245] The scattering anisotropy factor $\langle \cos\theta \rangle$ and photon mean free path $l = 1/(n_1 C_{ext})$ can be expressed as the functions of the Mie scattering coefficients a_n and b_n [Eqs. (6) and (7)]. Here, $n_1 (= \phi(\pi d^3/6))$ is the number density of scatterers. C_{ext} is the extinction cross section due to scattering and is given as

$$C_{ext} = 2\pi/k^2 \sum_{n=1}^{\infty} (2n+1)\text{Re}\{a_n + b_n\} \quad (5)$$

$$a_n = \frac{m'\psi_n(m'x)\psi_n'(x) - \mu\psi_n(x)\psi_n'(m'x)}{m'\psi_n(m'x)\varsigma_n'(x) - \mu\varsigma_n(x)\psi_n'(m'x)} \quad (6)$$

$$b_n = \frac{\mu\psi_n(m'x)\psi_n'(x) - m'\psi_n(x)\psi_n'(m'x)}{\mu\psi_n(m'x)\varsigma_n'(x) - m'\varsigma_n(x)\psi_n'(m'x)} \quad (7)$$

where $\psi_n(v) = v j_n(v)$ and $\varsigma_n(v) = v h_n^{(1)}(v)$ are the Ricatti-Bessel functions, $j_n(v)$ is spherical Bessel function of first kind of order n, $h_n^{(1)}(v)$ is spherical Hankel function of first kind of order n, $x = ka$ is the size parameter, $m' = N_1/N$, N_1 is the refractive index of the scatterer.

In the small particle limit and for magnetic scatterers, $|m'|ka \gg 1$ as $|\mu| \gg 1$. The anisotropy factor for lowest order term in ka is

$$\langle \cos\theta \rangle = \frac{\text{Re}(a_1 b_1^*)}{(|a_1|^2 + |b_1|^2)} \quad (8)$$

The periodic function $p(m', ka) = ka\tan(m'ka)$, which depends on μ, is responsible for the resonances in $\langle \cos\theta \rangle$. The appearance of such resonances in $\langle \cos\theta \rangle$ in the small particle limit ($ka \ll 1$) for magnetic scatterers ($\mu \neq 1$) are also shown by numerical means.[150] The presence of these resonances leads to an oscillatory behavior of localization parameter kl^* with μ. Thus, in the small particle limit, each single scattering event is characterized by

the presence of forward-backward asymmetry and resonance effects leading to a reduction of transport mean free path or the localization parameter. Whether the decrease of the localization parameter in the small particle limit for magnetic scatterers ($\mu \neq 1$) is responsible for the observed extinction of light? In the present experimental case, as the scattering of light takes place in the visible range of the spectrum, the scatterer μ should be unity. Therefore, the possibility of the decrease of transmitted light intensity due to the above mentioned mechanism can be ruled out.

As the magnetic field is increased, the sizes of scatterers increase due to the formation of doublets, triplets or very small chains, which change the scatterer's sizes i.e., the ka value drastically. Now, considering single scattering, the scattering anisotropy factor $\langle \cos \theta \rangle$ for spheres and extinction efficiency factor Q_{ext} for cylinders as a function of size parameter ka are analyzed in detail. The scattering anisotropy factor $\langle \cos \theta \rangle$ for a sphere of radius a is given as[246]

$$Q_{sca}\langle \cos \theta \rangle = \frac{4}{x^2}\left[\sum_n \frac{n(n+2)}{n+1}\mathrm{Re}\{a_n a_{n+1}^* + b_n b_{n+1}^*\} + \sum_n \frac{2n+1}{n(n+1)}\mathrm{Re}\{a_n b_n^*\} \right] \quad (9)$$

where $Q_{sca}(= C_{sca}/\pi a^2)$ is the scattering efficiency factor for a sphere. The scattering cross section C_{sca} can be expressed in terms of the Mie scattering coefficients a_n and b_n

$$C_{sca} = \frac{2\pi}{(ka)^2}\sum_{n=1}^{\infty}(2n+1)(|a_n|^2 + |b_n|^2) \quad (10)$$

Figure 7 shows the variation of scattering anisotropy factor $\langle \cos \theta \rangle$ as a function of size parameter ka for three different values of the magnetic permeability (μ) of the scatterer. Since we deal with scattering at optical frequency, the variation in $\langle \cos \theta \rangle$ for $\mu = 1$ is analyzed

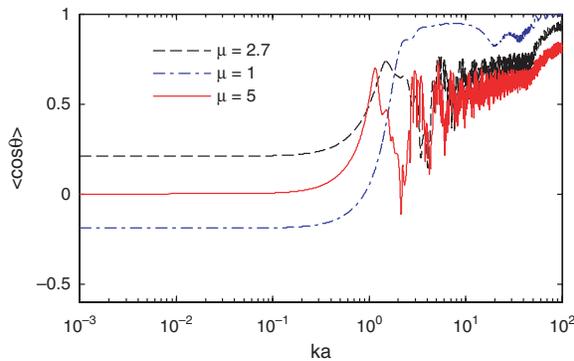in detail. For this case, the appearance of resonances in $\langle \cos \theta \rangle$ is observed as ka increases above some limit.

Another important quantity of interest in single scattering is the extinction efficiency factor, Q_{ext} which is defined as extinction cross section per unit length, c, divided by $2a$, the diameter of the cylinder. Physically, it represents the fraction of electromagnetic energy geometrically incident upon the particle which is abstracted from the beam. The extinction efficiency Q_{ext} of a cylinder when the cylinder axis lies in the plane determined by the propagation vector of the incident plane wave k, and the electric field E, is given as[247]

$$Q_{ext} = \frac{c_{E_{ext}}}{2a} = \frac{2}{ka}\mathrm{Re}\left\{ b_0^E + 2\sum_{n=1}^{\infty} b_n^E \right\} \quad (11)$$

where b_n^E is the scattering coefficient.

Figure 8 shows the behavior of Q_{ext}^E, as a function of size parameter ka for different incident angles (α) with the cylinder axis for an infinite cylinder with a refractive index 1.6 and magnetic permeability $\mu = 1$.[247] Since, the cylindrical structures formed in our dispersion are parallel to the incident light, α is close to zero. One of the interesting results in Figure 8 is the appearance of a large resonance peak in extinction efficiency factor Q_{ext}^E for an incidence angle $\alpha = 1°$, at size parameter value $ka = 0.663$.

The appearance and the origin of resonances in the scattering anisotropy factor $\langle \cos \theta \rangle$ for spheres and extinction efficiency factor Q_{ext}^E for cylinders have strong significance on scattering intensity. Analytically, the resonances in the scattering originate from a sharp minimum in the denominator of the corresponding scattering coefficients. The scattered electromagnetic wave arises from oscillations of electrons in the particle excited by the incident wave and can be imagined to have their origin in density distributions of oscillating electric and magnetic dipoles in the particle.[248] For the scattered electromagnetic wave, the electric wave arises from the electric dipoles and magnetic wave from the magnetic dipoles. The resonances

Fig. 7. Scattering anisotropy factor $\langle \cos \theta \rangle$ as function of size parameter ka for a sphere for different values of magnetic permeability (μ). Reprinted with permission from [41], J. M. Laskar, J. Philip, and B. Raj, *Phys. Rev. E* 78, 031404 (**2008**). © 2008, American Physical Society.
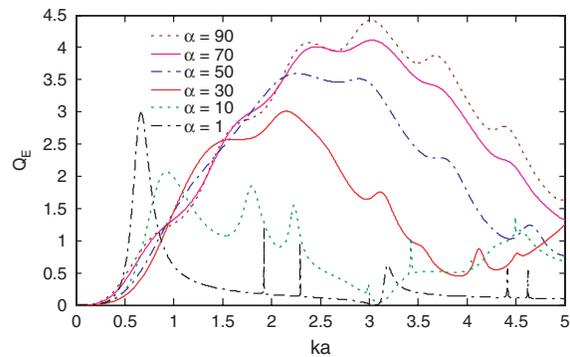

Fig. 8. Extinction efficiencies Q_{ext}^E as function of size parameter ka for different incident angles α for an infinite cylinder. Reprinted with permission from [41], J. M. Laskar, J. Philip, and B. Raj, *Phys. Rev. E* 78, 031404 (**2008**). © 2008, American Physical Society.

are related to the properties of the individual scattering coefficients, which in turn represent the amplitudes of the electric and magnetic multipoles excited within the particle. Therefore, physically the resonances correspond to the resonant excitation of a particular electric or magnetic multipole.

In the absence of any magnetic field, for a wavelength of 632.8 nm, and particle radius $a = 3.35$ nm, the average size parameter (ka) of the particles in the sample is ~ 0.033. As the external magnetic field is increased, the sizes of scatterers will increase due to the formation of doublets, triplets or very small chains, which changes the caterers size i.e., the ka value drastically. At the critical magnetic field H_{C_1}, some of the scatterers sizes are such that they satisfy the resonances in the scattering anisotropy factor and extinction efficiency factor. At the minimum transmitted intensity, the size distribution is such that the number of caterers that satisfy the resonance becomes maximum. Therefore, the resonances both in the scattering anisotropy factor and extinction efficiency factor, which physically correspond to resonant excitation of a particular electric or magnetic dipole within the scatterer, could be one of the plausible explanations for the observed extinction of light.

4.4. Origin of the Formation of Ring Structure in the Scattered Pattern

The reason for the formation of ring structure on the scattered pattern can be explained by considering scattering of light by a cylinder and evaluating the scattered electromagnetic field from cylindrical surface.[246] These scattered fields are derived for an infinite right circular cylinder of radius a when it is illuminated by a plane homogeneous wave $E_i = E_0 \exp(ik\hat{e}_i \cdot x)$. propagating in the direction $\hat{\mathbf{e}}_i = -\sin\zeta\hat{\mathbf{e}}_x - \cos\zeta\hat{\mathbf{e}}_z$ where ζ is the angle between the incident light wave and the cylinder axis. From the derived expressions for scattered electric field, it is inferred that the surfaces of constant phase, or wave fronts, of the scattered waves are the points which satisfy the condition

$$f(x, y, z) = r\sin\zeta - z\cos\zeta = C \qquad (12)$$

Therefore, the wave fronts are cones of half-angle ζ with their apexes at

$$z = -\frac{C}{\cos\zeta} \qquad (13)$$

The propagation of the scattered waves can be visualized as a cone that is sliding down the cylinder. The direction of propagation at any point on the cone, or wave normal $\hat{\mathbf{e}}_S$ is

$$\hat{\mathbf{e}}_S = \nabla f = \sin\zeta\hat{\mathbf{e}}_r - \cos\zeta\hat{\mathbf{e}}_z \qquad (14)$$

The Poynting vector is therefore, in the direction $\hat{\mathbf{e}}_S$. From Eqs. (9) and (10), it is clear that on placing a screen at some distance from the cylinder and perpendicular to the incident light, the resulting scattered pattern forms a conic section. When light is incident at near zero degree to the cylinder axis ($\zeta \approx 0°$), the scattered pattern is a circle. The evolution of the ring in the scattered pattern therefore clearly establishes the formation of such cylindrical rod like structures along the direction of propagation of the light wave above H_{C_2}, where the coupling constan $\Lambda \geq 1$. The diffused ring at lower magnetic fields indicates the distorted columns due to weak magnetic dipolar attraction. As the magnetic field increases, both the average chain length and the chain number increases. At higher fields, the ring becomes sharper indicating the formation of smooth surfaced columns as evident from the hexagonal symmetry.[40]

4.5. Transmitted Light Intensity at Different Critical Magnetic Fields

The time dependent variation of transmitted intensity and the scattered pattern indicates structural transitions at certain critical magnetic fields. Figure 9 shows the normalized transmitted intensity as a function of time required for the stabilization of intensity at different critical magnetic fields for a particular concentration of ferrofluid. The magnetic field values at which the temporal variation of transmitted intensity is observed are termed as the 'critical' fields. The transmitted intensity is normalized with respect to the absolute value of intensity in the absence of any magnetic field. At the critical fields, the intensity starts to decrease with time till it reaches a minimum value. After the minimum, the transmitted intensity again increases till its value gets saturated at a particular time. For all the concentrations of the sample, five 'critical' fields are observed as the magnetic field is increased up to 200 Gauss. Beyond the above mentioned value, the field could not be increased further due to overheating of the solenoid coil.
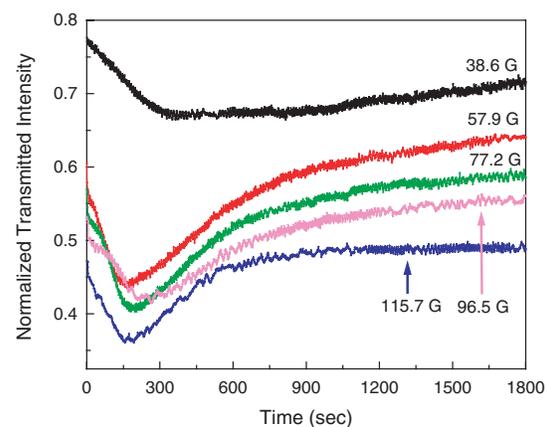

Fig. 9. Normalized transmitted intensity as a function of time required at different critical magnetic fields for a concentration ($\phi = 0.00819$) of ferrofluid. Reprinted with permission from [38], J. M. Laskar, J. Philip, and B. Raj, *Phys. Rev. E* 80, 041401 (**2009**). © 2009, American Physical Society.

At the first critical field, the particles start self assembling themselves as doublets, triplets, short chains and so on which increases the size of scatterers' in the system. The increase in length of the chains at a particular magnetic field is a time dependent process.[145] The reason for the decrease in the transmitted intensity due to the occurrence of resonance in the scattering efficiency resulting from the increase in scatterers size is discussed in detail previously. No variation either in the transmitted intensity till the first critical field confirms absence of aggregates. The length of the chains continues to increase with time at the first critical field until they attain the path length of the cell along the field direction. As time progresses, the gap between the chains also opens up with their increase in length. This causes the light transmission to increase again after reaching a minimum. The stabilization of the transmitted intensity confirms the completion of chain like structures that brings the system to equilibrium. Therefore, the time taken for the stabilization of transmitted intensity is the time required for the system to reach equilibrium at the first critical field.

While the transmitted intensity varies with time at the second critical field, structural rearrangement in the system takes place due to the lateral aggregation of the chains. After the transmitted intensity gets stabilized i.e., after the lateral aggregation of the chains, the system consists of columns of double chains distributed uniformly spanning the entire volume of the cell. This arrangement of uniform distribution of double chain columns in the system is retained till the external field is increased to the third one. Again, at the next critical field, these double chain columns undergo lateral aggregation (zippering) among themselves forming four chain columns. As the system comes to equilibrium by the above mentioned lateral aggregation of the columns, it consists of equally spaced uniformly distributed four chain columns. Again, there is no change in this distribution of columns in the cell until the next critical field is reached. The lateral aggregation of columns among themselves is again repeated at the fourth critical field forming eight chain columns. No variation in the transmitted intensity confirms the absence of any aggregation process between any two critical fields.

While the chains and columns undergo lateral aggregation at the second and higher critical fields, the fluctuation deviates the scattering surface from the cylindrical one and makes it rough. This fluctuation of the chains and columns also hinders the path of the light transmission. On reaching the equilibrium after the lateral aggregation, the fluctuation is minimized and more space opens up between the columns. This is the reason why the transmitted intensity first decreases and then increases after reaching a minimum.

4.6. Zippering Aggregation

It is important to know whether by undergoing lateral aggregation among the chains or columns from the second critical field onwards the potential energy of the system increases or decreases. While calculating the total system potential energy before and after aggregation at different critical fields, the chains and columns are assumed to be rigid. The potential energy between two chains can be calculated by summing the dipole–dipole interactions [Eq. (2)] between all the particles constituting the chains. For two rigid chains of magnetic colloids aligned parallel to one another, the interaction energy curve consists of two parts (1) an attractive energy well if the chains have a net attraction once they have zipped and (2) a repulsive interaction for parallel chains (of same length) as they approach one another laterally.[37, 154] When the chains are of different lengths or shifted with respect to one another (off registry), zippering of chains can take place due to attractive energy well. The lowest energy state of the system as predicted by the Gross model consists of clusters containing zipped chains.[154]

Figure 10 shows the form of interaction energy between two chains each containing 50 magnetic particles as function of their spacing for the first critical field and second critical field when the chains are in and out of registry. The alignment of particles under the above mentioned two conditions are shown in the inset of Figure 10. The magnitude of the energy barrier at the first critical field is $\sim 1.0 \times 10^{-23}$ Joule. At the second critical field when the magnetic field is increased by 20 Gauss, this energy barrier gets increased to $\sim 2.0 \times 10^{-23}$ Joule. The difference of these two energies is 1.0×10^{-23} Joule that is the exact energy required for the lateral aggregation of the two chains! This balance energy is used to overcome the energy barrier for

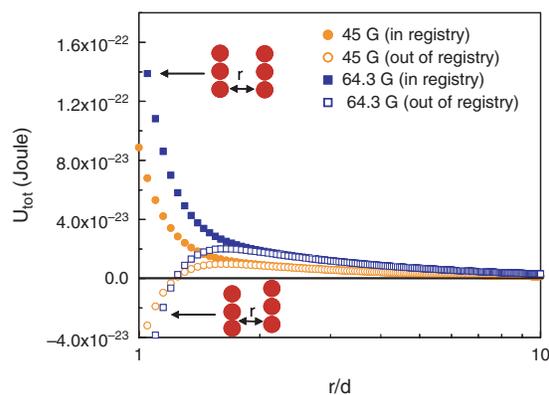**Fig. 10.** Interaction energy between two chains, each containing 50 magnetic particles, as function of their spacing at the first and second critical fields when the chains in and out of registry. The configuration of particles under the above two conditions are shown in the inset. Reprinted with permission from [38], J. M. Laskar, J. Philip, and B. Raj, *Phys. Rev. E* 80, 041401 (**2009**). © 2009, American Physical Society.

the lateral aggregation of the chains formed by the magnetic particles in presence of external magnetic. This is one of the plausible reasons for the occurrence of zippering at every 20 Gauss, above the first critical magnetic field. Since the system is continuously evolving under external magnetic field, it appears that the chains undergo a coarsening with time.

5. CONCLUSIONS

Ferrofluid exhibits very interesting optical properties in presence of applied magnetic field due to field assisted inter-particle interaction. On increasing applied field along the direction of chain formation, the transmitted intensity from a ferrofluid goes through a minimum followed by the appearance of a 'ring' like structure in the scattered pattern due to scattering anisotropy and dipolar resonances. The scattering from the cylindrical rod-like structures along the direction of light propagation gives rise to the formation of circular ring pattern. The zippering transitions of chains that are off-registry is manifested in the critical magnetic fields for minimal transmitted intensity. In brief, ferrofluid has been a wonderful model system for physicist to study interesting phenomena in tunable soft systems and have a variety of fascinating applications.

References and Notes

1. J. Jordanovic, S. Jäger, and S. H. L. Klapp, *Phys. Rev. Lett.* 106, 038301 (**2011**).
2. J. Philip, P. D. Shima, and B. Raj, *Appl. Phys. Lett.* 92, 043108 (**2008**).
3. P. D. Shima, J. Philip, and B. Raj, *Appl. Phys. Lett.* 95, 133112 (**2009**).
4. R. Massart, US Patent, 4329241 (**1982**).
5. R. Massart, E. Dubois, V. Cabuil, and E. Hasmonay, *J. Magn. Magn. Mater.* 149, 1 (**1995**).
6. G. Gnanaprakash, S. Ayyappan, T. Jayakumar, J. Philip, and B. Raj, *Nanotechnology* 17, 5851 (**2006**).
7. G. Gnanaprakash, J. Philip, T. Jayakumar, and B. Raj, *J. Phys. Chem. B* 111, 7978 (**2007**).
8. Y. P. He, Y. M. Miao, C. R. Li, S. Q. Wang, L. Cao, S. S. Xie, G. Z. Yang, B. S. Zou, and C. Burda, *Phys. Rev. B* 71, 125411 (**2005**).
9. B. D. Cullity, Introduction to Magnetic Materials, Addision-Wesley, New York (**1972**).
10. S. A. Oliver, H. H. Hamdeh, and J. C. Ho, *Phys. Rev. B* 60, 3400 (**1999**).
11. Q. A. Pankhurst, J. Connolly, S. K. Jones, and J. Dobson, *J. Phys. D: Appl. Phys.* 36, R167 (**2003**).
12. S. Bedanta and W. Kleemann, *J. Phys. D: Appl. Phys.* 42, 13001 (**2009**).
13. C. Kittel, *Mod. Phys.* 21, 541 (**1949**).
14. D. L. Leslie-Pelecky and R. D. Rieke, *Chem. Mater.* 8, 1770 (**1996**).
15. V. Cabuil, Preparation and properties of magnetic nanoparticles, Encyclopedia of Surface and Colloid Science, Marcel Dekker, New York (**2004**).
16. J. J. Chieh, S. Y. Yang, H. E. Horng, C. Y. Hong, and H. C. Yang, *Appl. Phys. Lett.* 90, 133505 (**2007**).
17. J. Philip, T. Jaykumar, P. Kalyanasundaram, and B. Raj, *Meas. Sci. Technol.* 14, 1289 (**2003**).
18. H. E. Horng, C. S. Chen, K. L. Fang, S. Y. Yang, J. J. Chieh, C. Y. Hong, and H. C. Yang, *Appl. Phys. Lett.* 85, 5592 (**2004**).
19. A. F. Bakuzis, K. S. Neto, P. P. Gravina, L. C. Figueiredo, P. C. Moraisa, L. P. Silva, R. B. Azevedo, and O. Silva, *Appl. Phys. Lett.* 84, 2355 (**2004**).
20. Y. Gao, J. P. Huang, Y. M. Liu, L. Gao, K. W. Yu, and X. Zhang, *Phys. Rev. Lett.* 104, 034501 (**2010**).
21. J. Philip, J. M. Laskar, and B. Raj, *Appl. Phys. Lett.* 92, 221911 (**2008**).
22. F. Leal-Calderon, T. Stora, O. M. Monval, and J. Bibette, *Phys. Rev. Lett.* 72, 2959 (**1994**).
23. J. Philip, G. G. Prakash, T. Jaykumar, P. Kalyanasundaram, and B. Raj, *Phys. Rev. Lett.* 89, 268301 (**2002**).
24. J. Philip, O. Mondain-Monval, F. L. Calderon, and J. Bibette, *J. Phys. D: Appl. Phys.* 30, 2798 (**1997**).
25. J. Philip, G. Gnanaprakash, T. Jaykumar, P. Kalyanasundaram, and B. Raj, *Macromolecules* 36, 9230 (**2003**).
26. J. Philip, G. Gnanaprakash, T. Jaykumar, P. Kalyanasundaram, and B. Raj, *Phys. Rev. Lett.* 89, 268301 (**2002**).
27. O. Mondain-Monval, F. L. Calderon, J. Philip, and J. Bibette, *Phys. Rev. Lett.* 75, 3364 (**1995**).
28. O. Mondain-Monval, A. Espert, P. Omarjee, J. Bibette, F. L. Calderon, J. Philip, and J. F. Joanny, *Phys. Rev. Lett.* 80, 1778 (**1998**).
29. J. Liu, E. M. Lawrence, A. Wu, M. L. Ivey, G. A. Flores, K. Javier, J. Bibette, and J. Richard, *Phys. Rev. Lett.* 74, 2828 (**1995**).
30. G. A. Flores, J. Liu, M. Mohebi, and N. Jamasbi, *Phys. Rev. E* 59, 751 (**1999**).
31. M. Fermigier and A. P. Gast, *J. Colloid Interface Sci.* 154, 522 (**1992**).
32. D. Wirtz and M. Fermigier, *Phys. Rev. Lett.* 72, 2294 (**1994**).
33. E. M. Furst and A. P. Gast, *Phys. Rev. E* 62, 6916 (**2000**).
34. A. J. Dickstein, S. Erramilli, R. E. Goldstein, D. P. Jackson, and S. A. Langer, *Science* 261, 1012 (**1993**).
35. R. M. Erb, H. S. Son, B. Samanta, V. M. Rotello, and B. B. Yellen, *Nature* 457, 999 (**2009**).
36. M. F. Islam, K. H. Lin, D. Lacoste, T. C. Lubensky, and A. G. Yodh, *Phys. Rev. E* 67, 021402 (**2003**).
37. R. Haghgooie and P. S. Doyle, *Phys. Rev. E* 75, 061406 (**2007**).
38. J. M. Laskar, J. Philip, and B. Raj, *Phys. Rev. E* 80, 041401 (**2009**).
39. M. Ivey, J. Liu, Y. Zhu, and S. Cutillas, *Phys. Rev. E* 63, 011403 (**2000**).
40. M. Klokkenburg, B. H. Erné, J. D. Meeldijk, and A. Wiedenmann, *Phys. Rev. Lett.* 97, 185702 (**2006**).
41. J. M. Laskar, J. Philip, and B. Raj, *Phys. Rev. E* 78, 031404 (**2008**).
42. M. T. A. Eloi, J. L. Santos, Jr, P. C. Morais, and A. F. Bakuzis, *Phys. Rev. E* 82, 021407 (**2010**).
43. R. E. Rosensweig, Ferrohydrodynamics, Dover Publications, Inc., New York (**1997**).
44. S. Odenbach, Ferrofluids: Magnetically Controllable Fluids and Their Applications, Springer, New York (**2003**).
45. E. Blūms, A. Cebers, and M. M. Maĭorov, Magnetic Fluids, Walter de Gruyter, Berlin (**1997**).
46. F. R. Arantes, A. M. F. Neto, and D. R. Cornejo, *J. Appl. Phys.* 109, 07E315 (**2011**).

47. H. Zhang and M. Widom, *Phys. Rev. E* 51, 2099 (**1995**).
48. K. I. Morozov, A. F. Pshenichinikoz, Y. L. Raikher, and M. I. Shliomis, *J. Magn. Magn. Mat.* 65, 269 (**1987**).
49. K. Zahn, J. M. Méndez-Alcaraz, and G. Maret, *Phys. Rev. Lett.* 79, 175 (**1997**).
50. B. Huke and M. Lucke, *Phys. Rev. E* 62, 6875 (**2000**).
51. A. O. Ivanov and O. B. Kuznetsova, *Phys. Rev. E* 64, 041405 (**2001**).
52. P. Jund, S. G. Kim, and C. Tsallis, *Phys. Rev. B* 52, 50 (**1995**).
53. B. Yellen, G. Friedman, and A. Feinerman, *J. Appl. Phys.* 91, 8552 (**2002**).
54. L. Y. Iskakova and A. Y. Zubarev, *Phys. Rev. E* 66, 041405 (**2002**).
55. B. B. Yellen and G. Friedman, *J. Appl. Phys.* 93, 8447 (**2003**).
56. Q. Fanyao and P. C. Morais, *J. Appl. Phys.* 93, 7385 (**2003**).
57. R. Toussaint, J. Akselvoll, G. Helgesen, A. T. Skjeltorp, and E. G. Flekkoy, *Phys. Rev. E* 60, 011407 (**2004**).
58. D. J. Klingenberg, J. C. Ulicny, and A. Smith, *Appl. Phys. Lett.* 86, 104101 (**2005**).
59. F. L. Calderon, T. Stora, O. M. Monval, P. Poulin, and J. Bibette, *Phys. Rev. Lett.* 72, 2959 (**1994**).
60. P. Poulin, V. Cabuil, and D. A. Weitz, *Phys. Rev. Lett.* 79, 4862 (**1997**).
61. L. C. Figueiredo, P. P. Gravina, K. S. Neto, P. C. Morais, L. P. Silva, R. B. Azevedo, M. Wagener, and N. Buske, *J. Appl. Phys.* 93, 8453 (**2003**).
62. X. Zhang, L. Liu, Y. Qi, Z. Liu, J. Shi, and W. Wen, *Appl. Phys. Lett.* 88, 134107 (**2006**).
63. A. F. Bakuzis, A. R. Pereira, J. G. Santos, and P. C. Morais, *J. Appl. Phys.* 99, 08C301 (**2006**).
64. C. J. Bae, S. Angappane, J. G. Parka, Y. Lee, J. Lee, K. An, and T. Hyeon, *Appl. Phys. Lett.* 91, 102502 (**2007**).
65. A. Wang, J. Li, and R. Gao, *Appl. Phys. Lett.* 94, 212501 (**2009**).
66. I. Hrianca, C. Caizer, and Z. Schlett, *J. Appl. Phys.* 92, 2125 (**2002**).
67. T. Jonsson, P. Svedlindh, and M. F. Hansen, *Phys. Rev. Lett.* 81, 3976 (**1998**).
68. V. P. Shilov, Y. L. Raikher, J.-C. Bacri, F. Gazeau, and R. Perzynski, *Phys. Rev. B* 60, 11902 (**1999**).
69. A. O. Ivanov, S. S. Kantorovich, E. N. Reznikov, C. Holm, A. F. Pshenichnikov, A. V. Lebedev, A. Chremos, and P. J. Camp, *Phys. Rev. E* 75, 061405 (**2007**).
70. P. P. Vaishnava, R. Tackett, A. Dixit, C. Sudakar, R. Naik, and G. Lawes, *J. Appl. Phys.* 102, 063914 (**2007**).
71. B. J. D. Gans, C. Blom, A. P. Philipse, and J. Mellema, *Phys. Rev. E* 60, 4518 (**1999**).
72. B. U. Felderhof, *Phys. Rev. E* 62, 3848 (**2000**).
73. Q. Li, Y. Xuan, and J. Wang, *Exp. Therm. Fluid Sci.* 30, 109 (**2005**).
74. W. F. Hall and S. N. Busenberg, *J. Chem. Phys.* 51, 137 (**1969**).
75. P. Ilg, M. Kröger, and S. Hess, *Phys. Rev. E* 71, 031205 (**2005**).
76. S. Y. Yang, Y. F. Chen, H. E. Horng, C. Y. Hong, W. S. Tse, and H. C. Yang, *Appl. Phys. Lett.* 81, 4931 (**2002**).
77. Y. F. Chen, S. Y. Yang, W. S. Tse, H. E. Horng, C. Y. Hong, and H. C. Yang, *Appl. Phys. Lett.* 82, 3481 (**2003**).
78. C. Y. Hong, S. Y. Yang, H. E. Horng, and H. C. Yang, *J. Appl. Phys.* 94, 3849 (**2003**).
79. S. L. Gomez, F. L. S. Cuppo, A. M. F. Neto, T. Kosa, M. Muramatsu, and R. J. Horowicz, *Phys. Rev. E* 59, 3059 (**1999**).
80. M. Liu, *Phys. Rev. Lett.* 80, 2937 (**1998**).
81. M. Liu, *Phys. Rev. E* 59, 3669 (**1999**).
82. P. A. Martinet, *Rheol. Acta* 13, 260 (**1974**).
83. Y. N. Skibin, V. V. Chekanov, and Y. L. Raizer, *Zh. Eksp. Teor. Fiz.* 72, 949 (**1977**).
84. H. W. Davies and J. M. Llewellyn, *J. Phys. D: Appl. Phys.* 13, 2327 (**1980**).
85. E. Blums, A. Cebers, and M. M. Maiorov, Magnetic Fluids, Walter de Gruyter, Berlin (**1997**).
86. Y. P. Chiu, Y. F. Chen, S. Y. Yang, J. C. Chen, H. E. Horng, H. C. Yang, W. S. Tse, and C. Y. Hong, *J. Appl. Phys.* 93, 2079 (**2003**).

87. A. Chaves, C. Rinaldi, S. Elborai, X. He, and M. Zahn, *Phys. Rev. Lett.* 96, 194501 (**2006**).
88. P. Ilg and M. Kröger, *Phys. Rev. E* 72, 031504 (**2005**).
89. S. Odenbach and H. Gilly, *J. Magn. Magn. Mater.* 152, 123 (**1996**).
90. S. Odenbach and H. Stork, *J. Magn. Magn. Mater.* 183, 188 (**1998**).
91. S. Odenbach, *J. Phys.: Condens. Matter* 15, S1497 (**2003**).
92. S. Odenbach, L. M. Pop, and A. Y. Zubarev, *GAMM-Mitteilungen* 30, 195 (**2007**).
93. A. M. F. Neto and M. M. F. Saba, *Phys. Rev. A* 34, 3483 (**1986**).
94. W. Luo, S. R. Nagel, T. F. Rosenbaum, and R. E. Rosensweig, *Phys. Rev. Lett.* 67, 2721 (**1991**).
95. B. Mertens, K. Levin, and G. S. Grest, *Phys. Rev. B* 49, 374 (**1994**).
96. T. Johnsson, J. Mattsson, C. Djurberg, F. A. Khan, P. Nordblad, and P. Svedlindh, *Phys. Rev. Lett.* 75, 4138 (**1995**).
97. D. P. Jackson and J. A. Miranda, *Phys. Rev. E* 67, 017301 (**2003**).
98. J. A. Miranda and R. M. Oliveira, *Phys. Rev. E* 69, 066312 (**2004**).
99. M. D. Cowley and R. E. Rosensweig, *J. Fluid. Mech.* 30, 671 (**1967**).
100. F. Petrelis, E. Falcon, and S. Fauve, *Eur. Phys. J. B* 15, 3 (**2000**).
101. G. Pacitto, C. Flament, J.-C. Bacri, and M. Widom, *Phys. Rev. E* 62, 7941 (**2000**).
102. Z. Huang, A. D. Luca, T. J. Atherton, M. Bird, C. Rosenblatt, and P. Carles, *Phys. Rev. Lett.* 99, 204502 (**2007**).
103. J. White, J. Oakley, M. Anderson, and R. Bonazza, *Phys. Rev. E* 81, 026303 (**2010**).
104. C.-Y. Chen, W.-L. Wu, and J. A. Miranda, *Phys. Rev. E* 82, 056321 (**2010**).
105. S. A. Langer, R. E. Goldstein, and D. P. Jackson, *Phys. Rev. A* 46, 4894 (**1992**).
106. D. P. Jackson, R. E. Goldstein, and A. O. Cebers, *Phys. Rev. E* 50, 298 (**1994**).
107. C.-Y. Chen, S.-Y. Wu, and J. A. Miranda, *Phys. Rev. E* 75, 036310 (**2007**).
108. P. G. Saffman and G. I. Taylor, *Proc. R. Soc. London* 245, 312 (**1958**).
109. F. Elias, C. Flament, and J.-C. Bacri, *Phys. Rev. Lett.* 77, 643 (**1996**).
110. S. Odenbach and M. Liu, *Phys. Rev. Lett.* 86, 328 (**2001**).
111. H. J. Pi, S. Park, J. Lee, and K. J. Lee, *Phys. Rev. Lett.* 84, 5316 (**2000**).
112. A. Engel, H. W. Muller, P. Reimann, and A. Jung, *Phys. Rev. Lett.* 91, 060602 (**2003**).
113. P. Rupp, R. Richter, and I. Rehberg, *Phys. Rev. E* 67, 036209 (**2003**).
114. R. Richter and V. Barashenkov, *Phys. Rev. Lett.* 94, 184503 (**2005**).
115. E. Bourdin, J.-C. Bacri, and E. Falcon, *Phys. Rev. Lett.* 104, 094502 (**2010**).
116. D. J. Korteweg and G. D. Vries, *Philos. Mag.* 39, 422 (**1895**).
117. R. Toussaint, E. G. Flekkøy, and G. Helgesen, *Phys. Rev. E* 74, 051405 (**2006**).
118. F. O. Boyer and E. Falcon, *Phys. Rev. Lett.* 103, 144501 (**2009**).
119. F. Boyer and E. Falcon, *Phys. Rev. Lett.* 101, 244502 (**2008**).
120. S. Dorbolo and E. Falcon, *Phys. Rev. E* 83, 046303 (**2011**).
121. C. Sena, M. H. Godinho, and A. M. F. Neto, *J. Appl. Phys.* 102, 073524 (**2007**).
122. M. F. D. Silva and A. M. F. Neto, *Phys. Rev. E* 48, 4483 (**1993**).
123. T.-Z. Zhang, J. Li, H. Miao, Q.-M. Zhang, J. Fu, and B.-C. Wen, *Phys. Rev. E* 82, 021403 (**2010**).
124. J. M. Laskar, J. Philip, and B. Raj, *Phys. Rev. E* 82, 021402 (**2010**).
125. H. Bhatt, R. Patel, and R. V. Mehta, *J. Opt. Soc. Am. A* 27, 873 (**2010**).
126. C. Rablau, P. Vaishnava, C. Sudakar, R. Tackett, G. Lawes, and R. Naik, *Phys. Rev. E* 78, 051502 (**2008**).
127. D. Soga, S. Alves, A. Campos, F. A. Tourinho, J. Depeyrot, and A. M. F. Neto, *J. Opt. Soc. Am. B* 24, 49 (**2007**).
128. S. John, *Phys. Rev. Lett.* 53, 2169 (**1984**).

129. D. S. Wiersma, P. Bartolini, A. Lagendijk, and R. Righini, *Nature* 390, 671 (**1997**).

130. P. Sheng, Scattering and Localization of Classical Waves in Random Media, World Scientific, Singapore (**1990**).

131. Y. Kuga and A. Ishimaru, *J. Opt. Soc. Am. A* 8, 831 (**1984**).

132. M. P. V. Albada and A. Lagendijk, *Phys. Rev. Lett.* 55, 2692 (**1985**).

133. J. D. Joannopoulos, R. D. Meade, and J. N. Winn, Photonic Crystals, Princeton University Press, Princeton (**1995**).

134. S. Haroche and D. Kleppner, *Phys. Today* 24, 42 (**1989**).

135. E. Betzig and J. K. Trautman, *Science* 257, 189 (**1992**).

136. D. Lacoste, F. Donatini, S. Neveu, J. A. Serughetti, and B. A. V. Tiggelen, *Phys. Rev. E* 62, 3934 (**2000**).

137. R. V. Mehta, R. Patel, R. Desai, R. V. Upadhyay, and K. Parekh, *Phys. Rev. Lett.* 96, 127402 (**2006**).

138. R. V. Mehta, R. Patel, and R. V. Upadhyay, *Phys. Rev. B* 74, 195127 (**2006**).

139. J. E. Martin, K. M. Hill, and C. P. Tigges, *Phys. Rev. E* 59, 5676 (**1999**).

140. K. T. Wu, Y. D. Yao, C. R. C. Wang, P. F. Chen, and E. T. Yeh, *J. Appl. Phys.* 85, 5959 (**1999**).

141. T. Du and W. Luo, *J. Appl. Phys.* 85, 5953 (**1999**).

142. T. Du and W. Luo, *Appl. Phys. Lett.* 72, 272 (**1998**).

143. J. Li, X. Liu, Y. Lin, L. Bai, Q. Li, X. Chen, and A. Wang, *Appl. Phys. Lett.* 91, 253108 (**2007**).

144. T. Klein, A. Laptev, A. Günther, P. Bender, A. Tschöpe, and R. Birringer, *J. Appl. Phys.* 106, 114301 (**2009**).

145. F. Martinez-Pedredo, A. El-Harrak, J. C. Fernandez-Tolenado, M. Tirado-Miranda, J. Baudry, A. Schmitt, J. Bibette, and J. C. Fernandez, *Phys. Rev. E* 78, 011403 (**2008**).

146. F. M. Pedredo, M. T. Miranda, A. Schmitt, and J. C. Fernandez, *J. Chem. Phys.* 125, 084706 (**2006**).

147. W. D. Young and D. C. Prieve, *Ind. Eng. Chem. Res.* 35 3186 (**1996**).

148. J. J. M. Janssen, J. J. M. Baltussen, A. P. V. Gelder, and J. A. A. J. Prenboom, *J. Phys. D: Appl. Phys.* 23, 1447 (**1990**).

149. M. Kerker, D. S. Wang, and C. L. Giles, *J. Opt. Soc. Am.* 73, 765 (**1983**).

150. F. A. Pinheiro, A. S. Martinez, and L. C. Sampaio, *Phys. Rev. Lett.* 84, 1435 (**2000**).

151. F. A. Pinheiro, A. S. Martinez, and L. C. Sampaio, *Phys. Rev. Lett.* 85, 5563 (**2000**).

152. K. Parekha, R. Patel, R. V. Upadhyay, and R. V. Mehta, *J. Magn. Magn. Mater.* 289, 311 (**2005**).

153. H. Reerink and J. Th. G. Overbeek, *Disc. Fraday Soc.* 18, 74 (**1954**).

154. M. Gross, *Phys. Rev. E* 58, 6124 (**1998**).

155. J. Promislow, A. P. Gast, and M. Fermigier, *J. Chem. Phys.* 102, 5492 (**1995**).

156. G. Helgesen, A. T. Skjeltorp, P. M. Mors, R. Botet, and R. Jullien, *Phys. Rev. Lett.* 61, 1736 (**1988**).

157. M. C. Miguel and R. Pasto-Satorras, *Phys. Rev. E* 59, 826 (**1999**).

158. G. Bossis, C. Mathis, Z. Minouni, and C. Paparoditis, *Europhys. Lett.* 11, 133 (**1990**).

159. D. Sohn, *J. Magn. Magn. Mater.* 173, 305 (**1997**).

160. J. Cernak, P. Macko, and M. Kasparkova, *J. Phys. D* 24, 1609 (**1991**).

161. J. Cernak, *J. Magn. Magn. Mater.* 132, 258 (**1994**).

162. J. E. Martin, J. Odinek, and T. C. Halsey, *Phys. Rev. Lett.* 69, 1524 (**1992**).

163. S. Melle, M. A. Rubio, and G. G. Fuller, *Phys. Rev. Lett.* 87, 115501 (**2001**).

164. P. D. Duncan and P. J. Camp, *J. Chem. Phys.* 121, 11322 (**2004**).

165. P. D. Duncan and P. J. Camp, *Phys. Rev. Lett.* 97, 107202 (**2006**).

166. T. Ukai and T. Maekawa, *Phys. Rev. E* 69, 032501 (**2004**).

167. M. Mohebi, N. Jamasbi, and J. Liu, *Phys. Rev. E* 54, 5407 (**1996**).

168. D. Heinrich, A. R. Goni, and C. Thomsen, *J. Chem. Phys.* 126, 124701 (**2007**).

169. A. Wiedenmann, U. Keiderling, K. Habicht, M. Russina, and R. Gahler, *Phys. Rev. Lett.* 97, 057202 (**2006**).

170. J. E. Martin, R. A. Anderson, and C. P. Tigges, *J. Chem. Phys.* 108, 3765 (**1998**).

171. A.-P. Hynninen and M. Dijkstra, *Phys. Rev. Lett.* 94, 138303 (**2005**).

172. J. Jordanovic and S. H. L. Klapp, *Phys. Rev. Lett.* 101, 038302 (**2008**).

173. C.-H. Chang, C.-W. Tan, J. Miao, and G. Barbastathis, *Nanotechnology* 20, 495301 (**2009**).

174. S. H. Lee and C. M. Liddell, *Small* 5, 1957 (**2009**).

175. S. Odenbach, Colloidal Magnetic Fluids: Basics, Development and Application of Ferrofluids, Springer-Verlag, Berlin, Hiedelberg (**2009**).

176. F. Wiekhorst, U. Steinhoff, D. Eberbeck, and L. Trahms, *Pharm. Res.* 29, 1189 (**2012**).

177. K. Raj and R. Moskowitz, *J. Magn. Magn. Mater.* 85, 233 (**1990**).

178. N. Saga and T. Nakamura, *J. Appl. Phys.* 91, 7003 (**2002**).

179. C. Goubault, P. Jop, M. Fermigier, J. Baudry, E. Bertrand, and J. Bibette, *Phys. Rev. Lett.* 91, 260802 (**2003**).

180. J. Philip, C. B. Rao, T. Jayakumar, and B. Raj, *NDT and E Int.* 33, 289 (**2000**).

181. V. Mahendran and J. Philip, *Appl. Phys. Lett.* 100, 073104 (**2012**).

182. J. Hesselbach and C. Abel-Keilhack, *J. Appl. Phys.* 93, 8441 (**2003**).

183. N. Pekas, M. D. Porter, M. Tondra, A. Popple, and A. Jander, *Appl. Phys. Lett.* 85, 4783 (**2004**).

184. D. W. Inglis, R. Riehn, R. H. Austin, and J. C. Sturm, *Appl. Phys. Lett.* 85, 5093 (**2004**).

185. Y. Melikhov, S. J. Lee, D. C. Jiles, D. H. Schmidt, M. D. Porter, and R. Shinar, *J. Appl. Phys.* 93, 8438 (**2003**).

186. R. Ravaud, G. Lemarquand, and V. Lemarquand, *J. Appl. Phys.* 106, 034911 (**2009**).

187. S. Pu, X. Chen, L. Chen, W. Liao, Y. Chen, and Y. Xia, *Appl. Phys. Lett.* 87, 021901 (**2005**).

188. S. S. Nair, J. Thomas, C. S. S. Sandeep, M. R. Anantharaman, and R. Philip, *Appl. Phys. Lett.* 92, 171908 (**2008**).

189. S. Pu, X. Chen, Z. Di, and Y. Xia, *J. Appl. Phys.* 101, 053532 (**2007**).

190. F. Choueikani, F. Royer, D. Jamon, A. Siblini, J. J. Rousseau, S. Neveu, and J. Charara, *Appl. Phys. Lett.* 94, 051113 (**2009**).

191. T. Liu, X. Chen, Z. Di, J. Zhang, X. Li, and J. Chen, *Appl. Phys. Lett.* 91, 121116 (**2007**).

192. W. Liao, X. Chen, Y. Chen, S. Pu, Y. Xia, and Q. Li, *Appl. Phys. Lett.* 87, 151122 (**2005**).

193. M. Strömberg, K. Gunnarsson, S. Valizadeh, P. Svedlindha, and M. Strømme, *J. Appl. Phys.* 101, 023911 (**2007**).

194. S. H. Chung, A. Hoffmann, S. D. Bader, C. Liu, B. Kay, L. Makowski, and L. Chen, *Appl. Phys. Lett.* 85, 2971 (**2004**).

195. R. Kappiyoor, M. Liangruksa, R. Ganguly, and I. K. Puri, *J. Appl. Phys.* 108, 094702 (**2010**).

196. D. Serantes, D. Baldomir, C. Martinez-Boubeta, K. Simeonidis, M. Angelakeris, E. Natividad, M. Castro, A. Mediano, D.-X. Chen, A. Sanchez, L. Balcells, and B. Martínez, *J. Appl. Phys.* 108, 073918 (**2010**).

197. Y. Huang, J. H. Kim, S. I. Park, H. Shao, and C. O. Kim, *J. Appl. Phys.* 93, 8444 (**2003**).

198. P. P. Macaroff, A. R. Simioni, Z. G. M. Lacava, E. C. D. Lima, P. C. Morais, and A. C. Tedesco, *J. Appl. Phys.* 99, 08S102 (**2006**).

199. J.-B. Mathieu and S. Martel, *J. Appl. Phys.* 106, 044904 (**2009**).

200. D. Eberbeck, F. Wiekhorst, U. Steinhoff, and L. Trahms, *Appl. phys. Lett.* 95, 213701 (**2009**).

201. D. Eberbeck, F. Wiekhorst, S. Wagner, and L. Trahms, *Appl. Phys. Lett.* 98, 182502 (**2011**).

202. D. Brousseau, E. F. Borra, H. Jean-Ruel, J. Parent, and A. Ritcey, *Opt. Express* 14, 11486 (**2006**).

REVIEW

REVIEW

203. D. Brousseau, E. F. Borra, and S. Thibault, *Opt. Express* 15, 18190 (**2007**).

204. D. Brousseau, E. F. Borra, M. Rochette, and D. B. Landry, *Opt. Express* 18, 8239 (**2010**).

205. G. V. Kurlyandskaya, M. L. Sánchez, B. Hernando, V. M. Prida, P. Gorria, and M. Tejedor, *Appl. Phys. Lett.* 82, 3053 (**2003**).

206. H. E. Horng, C. Y. Hong, S. Y. Yang, and H. C. Yang, *Appl. Phys. Lett.* 82, 2434 (**2003**).

207. C. Y. Hong, W. S. Chen, Z. F. Jian, S. Y. Yang, H. E. Horng, L. C. Yang, and H. C. Yang, *Appl. Phys. Lett.* 90, 074105 (**2007**).

208. R. Patel and A. Raval, *Appl. Phys. Lett.* 90, 254104 (**2007**).

209. W. B. Song, Z. Ding, C. Son, and B. Ziaie, *Appl. Phys. Lett.* 90, 092501 (**2007**).

210. A. Winkleman, K. L. Gudiksen, D. Ryan, G. M. Whitesides, D. Greenfield, and M. Prentiss, *Appl. Phys. Lett.* 85, 2411 (**2004**).

211. S. Pu, X. Chen, Y. Chen, W. Liao, L. Chen, and Y. Xia, *Appl. Phys. Lett.* 86, 171904 (**2005**).

212. S. Pu, X. Chen, L. Chen, W. Liao, Y. Chen, and Y. Xia, *Appl. Phys. Lett.* 87, 021905 (**2005**).

213. C. Y. Hong, C. C. Wu, Y. C. Chiu, S. Y. Yang, H. E. Horng, and H. C. Yang, *Appl. Phys. Lett.* 88, 212512 (**2006**).

214. Z. G. Guo, F. Zhou, J. C. Hao, Y. M. Liang, W. M. Liu, and W. T. S. Huck, *Appl. Phys. Lett.* 89, 081911 (**2006**).

215. Q. L. Ye, H. Yoshikawa, S. Bandow, and K. Awaga, *Appl. Phys. Lett.* 94, 063114 (**2009**).

216. T. Kruse, H.-G. Krauthäuser, A. Spanoudaki, and R. Pelster, *Phys. Rev. B* 67, 094206 (**2003**).

217. A. Wiedenmann, U. Keiderling, M. Meissner, D. Wallacher, R. Gähler, R. P. May, S. Prévost, M. Klokkenburg, B. H. Erné, and J. Kohlbrecher, *Phys. Rev. B* 77, 184417 (**2008**).

218. A. V. Teixeira, I. Morfin, F. Ehrburger-Dolle, C. Rochas, E. Geissler, P. Licinio, and P. Panine, *Phys. Rev. E* 67, 021504 (**2003**).

219. M. Klokkenburg, B. H. Erné, A. Wiedenmann, A. V. Petukhov, and A. P. Philipse, *Phys. Rev. E* 75, 051408 (**2007**).

220. A. Wiedenmann, A. Hoell, M. Kammel, and P. Boesecke, *Phys. Rev. E* 68, 031203 (**2003**).

221. R. Pynn, J. B. Hayter, and S. W. Charles, *Phys. Rev. Lett.* 51, 710 (**1983**).

222. B. J. Lemaire, P. Davidson, P. Panine, and J. P. Jolivet, *Phys. Rev. Lett.* 93, 267801 (**2004**).

223. R. Chantrell, A. Bradbury, J. Popplewell, and S. W. Charles, *J. Phys. D* 13, L119 (**1980**).

224. R. Chantrell, A. Bradbury, J. Popplewell, and S. W. Charles, *J. Appl. Phys.* 53, 2742 (**1982**).

225. S. Menear, A. Bradbury, and R. Chantrell, *J. Magn. Magn. Mater.* 43, 166 (**1984**).

226. D. Q. Wei and G. N. Patey, *Phys. Rev. Lett.* 68, 2043 (**1992**).

227. J. J. Weis and D. Levesque, 71, 2729 (**1993**).

228. M. J. Stevens and G. S. Grest, *Phys. Rev. Lett.* 72, 3686 (**1994**).

229. M. J. Stevens and G. S. Grest, *Phys. Rev. E* 51, 5962 (**1995**).

230. S. W. Davis, W. McCausland, H. C. McGahagan, C. T. Tanaka, and M. Widom, *Phys. Rev. E* 59, 2424 (**1999**).

231. P. J. Camp and G. N. Patey, *Phys. Rev. E* 62, 5403 (**2000**).

232. V. V. Murashov, P. J. Camp, and G. N. Patey, *J. Chem. Phys.* 116, 6731 (**2002**).

233. A. F. Pshenichnikov and V. Mekhonoshin, *Eur. Phys. J. E* 6, 399 (**2001**).

234. T. Kruse, A. Spanoudaki, and R. Pelster, *Phys. Rev. B* 68, 054208 (**2003**).

235. J. Richardi and M. P. Pileni, *Phys. Rev. E* 77, 061510 (**2008**).

236. P. Jund, S. G. Kim, D. Tomanek, and J. Hetherington, *Phys. Rev. Lett.* 74, 3049 (**1995**).

237. C. F. Hayes, *J. Colloid Interface Sci.* 52, 239 (**1975**).

238. H. Wang, Y. Zhu, C. Boyd, W. Luo, A. Cebers, and R. E. Rosensweig, *Phys. Rev. Lett.* 72, 1929 (**1994**).

239. W.-X. Fang, Z.-H. He, X.-Q. Xu, Z.-Q. Mao, and H. Shen, *Europhys. Lett.* 77, 68004 (**2007**).

240. J. Wu, M. Aslam, and V. P. Dravid, *Appl. Phys. Lett.* 93, 082505 (**2008**).

241. B. Hoffmann and W. Kohler, *J. Magn. Magn. Mater.* 262, 289 (**2003**).

242. V. Joudrier, P. Bourdon, F. Hache, and C. Flytzanis, *Appl. Phys. B: Lasers Opt.* 67, 627 (**1998**).

243. C. Christiansen, *Ann. Phys.* 23, 298 (**1884**).

244. G. L. Fischer, R. W. Boyd, T. R. Moore, and J. E. Sipe, *Opt. Lett.* 21, 1643 (**1996**).

245. B. A. V. Tiggelen, *Phys. Rev. Lett.* 75, 422 (**1995**).

246. C. F. Bohren and D. R. Huffman, Absorption and Scattering of Light by Small particles, Wiley-Interscience, John Wiley & Sons, New York (**1983**).

247. A. C. Lind and J. M. Greenberg, *J. Appl. Phys.* 37, 3195 (**1966**).

248. M. Kerker, The Scattering of Light and Other Electromagnetic Radiation, Academic Press, New York and London (**1969**).